AGU PUBLICATIONS

JGR

Journal of Geophysical Research: Atmospheres

RESEARCH ARTICLE
10.1002/2017JD027141

Key Points:
- ARM observational data are used to estimate the terrestrial component of land-atmosphere coupling strength in the U.S. SGP region
- Both free-running and constrained climate model simulations of regional atmospheric coupling with soil moisture are too strong
- Simulated coupling of local vegetation leaf area with surface evaporative fraction is weaker than the observational estimate

Supporting Information:
- Supporting Information S1

Correspondence to:
T. J. Phillips,
phillips14@llnl.gov

Citation:
Phillips, T. J., Klein, S. A., Ma, H.-Y., Tang, Q., Xie, S., Williams, I. N., … Torn, M. S. (2017). Using ARM observations to evaluate climate model simulations of land-atmosphere coupling on the U.S. Southern Great Plains. *Journal of Geophysical Research: Atmospheres, 122*. https://doi.org/10.1002/2017JD027141

Received 15 MAY 2017
Accepted 8 OCT 2017
Accepted article online 13 OCT 2017

Using ARM Observations to Evaluate Climate Model Simulations of Land-Atmosphere Coupling on the U.S. Southern Great Plains

Thomas J. Phillips[1], Stephen A. Klein[1], Hsi-Yen Ma[1], Qi Tang[1], Shaocheng Xie[1], Ian N. Williams[2], Joseph A. Santanello[3], David R. Cook[4], and Margaret S. Torn[2]

[1]Lawrence Livermore National Laboratory, Livermore, CA, USA, [2]Lawrence Berkeley National Laboratory, Berkeley, CA, USA, [3]NASA Goddard Space Flight Center Hydrological Sciences Laboratory, Greenbelt, MD, USA, [4]Argonne National Laboratory, Lemont, IL, USA

Abstract Several independent measurements of warm-season soil moisture and surface atmospheric variables recorded at the ARM Southern Great Plains (SGP) research facility are used to estimate the terrestrial component of land-atmosphere coupling (LAC) strength and its regional uncertainty. The observations reveal substantial variation in coupling strength, as estimated from three soil moisture measurements at a single site, as well as across six other sites having varied soil and land cover types. The observational estimates then serve as references for evaluating SGP terrestrial coupling strength in the Community Atmospheric Model coupled to the Community Land Model. These coupled model components are operated in both a free-running mode and in a controlled configuration, where the atmospheric and land states are reinitialized daily, so that they do not drift very far from observations. Although the controlled simulation deviates less from the observed surface climate than its free-running counterpart, the terrestrial LAC in both configurations is much stronger and displays less spatial variability than the SGP observational estimates. Preliminary investigation of vegetation leaf area index (LAI) substituted for soil moisture suggests that the overly strong coupling between model soil moisture and surface atmospheric variables is associated with too much evaporation from bare ground and too little from the vegetation cover. These results imply that model surface characteristics such as LAI, as well as the physical parameterizations involved in the coupling of the land and atmospheric components, are likely to be important sources of the problematical LAC behaviors.

1. Introduction

Land-atmosphere coupling (LAC) has important implications for weather and climate predictability, as well as the simulation of climatic change (Orth & Seneviratne, 2017; Seneviratne et al., 2010). The past 15 years have witnessed numerous studies focusing on the coupling between soil moisture and diverse variables of the atmospheric boundary layer, as displayed by models, reanalyses, and observations.

Early LAC numerical experimentation utilized single models (Dirmeyer, 2001) but quickly advanced to execution of systematic intercomparison experiments involving multiple global climate models (GCMs) (Koster et al., 2002, 2004, 2006, 2010, 2011). These GCM studies promoted the concept of "hot spots," located in semiarid zones such as the U.S. Great Plains. Here the interactions of summertime soil moisture with surface temperature and humidity, and potentially also with precipitation mediated by local convection, are especially strong (Gentine et al., 2013; Guo et al., 2006; Tawfik et al., 2015a, 2015b; Taylor et al., 2012). In such moisture-limited regions—and especially in summer when radiative warming of the land is high—surface evaporation, humidity, and temperature are strongly influenced by soil moisture, and thus, LAC tends to be most intense.

The GCM intercomparisons inspired a subsequent wave of numerical experimentation focusing on details of LAC on different continents, which sometimes also employed mesoscale atmospheric models or regional climate models (e.g., Comer & Best, 2012; Dirmeyer et al., 2012; Diro et al., 2014; Fischer et al., 2007; Guo & Dirmeyer, 2013; Hirsch et al., 2016; Hirsch et al., 2014; Lawrence & Slingo, 2005; Lorenz et al., 2012; Lorenz et al., 2015; Mei & Wang, 2012; Meng & Quiring, 2010; Santanello, Peters-Lidard et al., 2011; Santanello et al., 2007; Santanello et al., 2009, 2013; Seneviratne et al., 2006; Sun & Pritchard, 2016; Wei et al., 2010). In addition, large-scale LAC was diagnosed in multiple climate models participating in the Coupled Model

Intercomparison Project (CMIP) (Dirmeyer et al., 2013; Notaro, 2008; Williams et al., 2012), which also included specialized experiments with prescribed versus prognostic soil moisture (Berg et al., 2015; Seneviratne et al., 2013). More recently, modeling studies by Koster et al. (2016) and Zhou et al. (2016) highlighted remote interactions of soil moisture anomalies with the large-scale atmospheric circulation over North America.

As with free-running modeling experiments, reanalyses offer an opportunity to study LAC at continental to global scales, but with simulations that are steadily updated by assimilating available observations. Examples of this approach include work by Ruiz-Barradas and Nigam (2006), Luo et al. (2006), Wei and Dirmeyer (2010, 2012), Findell et al. (2011), Song et al. (2016), and Santanello et al. (2015). In some instances also, LAC in several different reanalyses was compared with that in global or regional models (e.g., Liu et al., 2014; Zeng et al., 2010).

Unrealistic representations of LAC that are attributable to the models underlying the reanalyses (e.g., Santanello et al., 2015) have motivated alternative investigations using available observations. These include satellite-based investigation of large-scale LAC (Ferguson & Wood, 2011; Ferguson et al., 2012; Levine et al., 2016; Tuttle & Salvucci, 2016), local or regional-scale LAC estimated from in situ field observations (Dirmeyer et al., 2006; Ford et al., 2017; Ford, Rapp, Quiring, 2015; Ford, Rapp, Quiring, Blake, 2015; Guillod et al., 2014, 2015; Kustas et al., 2005; Lamb et al., 2012; Phillips & Klein, 2014; Ruiz-Barradas & Nigam, 2013; Santanello et al., 2005), or a mixture of both approaches (Miralles et al., 2012; Roundy & Santanello, 2017). Many in situ observational analyses have employed extensive data records suitable for LAC studies that are maintained by the U.S. Department of Energy Atmospheric Radiation Measurement (ARM) and AmeriFlux Programs (Hargrove et al., 2003; Mather & Voyles, 2013). In particular, the ARM Southern Great Plains (SGP) facilities in Northern Oklahoma and Southern Kansas (Berg & Lamb, 2016; Sisterson et al., 2016) have provided the continuous data records required for investigations of LAC in a hot spot region.

A few common themes run through results of the historical collection of modeling, reanalysis, and observational studies. One is that the coupling of soil moisture with surface atmospheric variables such as evaporation or temperature is generally more robust than its coupling with local precipitation via convective processes. Indeed, the extent to which soil moisture significantly impacts precipitation in different locations still remains unresolved, despite receiving much scientific attention (e.g., Findell et al., 2011; 2015; Ford, Quiring et al., 2015; Ford, Rapp, Quiring, 2015; Ford, Rapp, Quiring, Blake, 2015; Guillod et al., 2014, 2015; Lamb et al., 2012; Phillips & Klein, 2014; Ruiz-Barradas & Nigam, 2013; Taylor et al., 2012; Tuttle & Salvucci, 2016). A conceptual framework for addressing the coupling of soil moisture with precipitation is to view this as a two-legged process: a *terrestrial* component involving soil moisture coupling with surface evaporation, and an *atmospheric* linkage between surface evaporation and convective precipitation (Dirmeyer, 2011; Santanello, Ferguson et al., 2011; Tawfik et al., 2015a, 2015b). Where model results have been compared with reanalyses or observations (e.g., Dirmeyer et al., 2006; Ferguson et al., 2012; Levine et al., 2016; Phillips & Klein, 2014; Ruiz-Barradas & Nigam, 2006; Zeng et al., 2010), a second common theme is that simulated coupling of soil moisture with atmospheric variables is generally too strong, although this may depend on model-specific parameterizations (Comer & Best, 2012; Lawrence & Slingo, 2005; Mei & Wang, 2012; Sun & Pritchard, 2016).

Further investigation of the putative overly strong model representation of coupling strength motivates the present study, which focuses solely on the terrestrial link in the soil moisture-atmospheric coupling chain. This focus ensures that a truly *local* estimate of the LAC strength is obtained: if the atmospheric linkage were also to be investigated, effects on the 10–50 km mesoscale would need to be taken into account.

Our study employs ARM in situ measurements in the SGP region to evaluate terrestrial LAC in version 5.1 of the Community Atmospheric Model coupled to version 4 of the Community Land Model (Neale et al., 2012; Oleson et al., 2010). While the scarcity of in situ soil moisture (SM) measurements often hinders reliable estimation of observed LAC, there exist three independent data sets of shallow-depth SM, as well as alternative measurements of surface atmospheric variables (e.g., latent/sensible heat fluxes, relative humidity, temperature) at the Central Facility (CF) of the ARM Southern Great Plains site near Lamont, Oklahoma (at coordinates 36.61° north latitude and 97.48° west longitude). In addition, there are other SM and atmospheric measurements at ARM sites surrounding the CF that are sufficient to allow estimation of terrestrial LAC in the SGP region. Of course, diverse measurements of local soil moisture and surface atmospheric variables in the context of varying soil types and vegetation covers are expected to give rise to different estimates of

terrestrial LAC strength. These strength differences provide a rough measure of the inherent uncertainties existing in various aspects of the regional-scale LAC and thus supply a reference standard for evaluating similar LAC aspects simulated by the climate model.

Most previous modeling studies of LAC have employed simulations where both the atmospheric and land components are initialized from model-specific climatologies, and where soil moisture and temperature are spun-up until a quasi-equilibrium coupled climate state is achieved. Subsequent numerical integration then usually proceeds with observed historical variations in ocean sea surface temperatures (SSTs) and sea ice extents prescribed, as in standard Atmospheric Model Intercomparison Project (AMIP) experiments (Gates et al., 1999).

Our study also evaluates terrestrial LAC in such a free-running AMIP simulation of the CAM5.1/CLM4 model. In addition, we make use of a continuous chain of CAM5.1 hindcasts in which the atmospheric and land states are kept close to observations (Ma et al., 2015). Running the CAM5.1/CLM4 coupled system in such a controlled hindcast (HC) configuration has the distinct advantage of mitigating biases introduced by the modeled atmospheric dynamics, in order to highlight errors that are more closely tied to the model's parameterized physical processes (Phillips et al., 2004). Hence, a central focus of our study is to identify differences in the strength and characteristics of land-atmosphere coupling that are displayed by the CAM5.1/CLM4 when it is run in the free-running AMIP versus the controlled HC configuration.

The remainder of this paper is organized as follows. Section 2 describes the pertinent measurements of soil moisture and surface atmospheric variables available at the SGP-CF site, and section 3 includes discussion of the analysis approach and the metrics used for estimating coupling strength, as well as the range of LAC results at both the CF site and over the broader SGP region. In section 4, the implementations of the free-running AMIP versus controlled HC configurations of the coupled CAM5/CLM4 model are discussed. Their respective simulations of terrestrial LAC are evaluated relative to the range of SGP observational estimates in section 5, and a general validation of surface variables in both the AMIP and HC simulations is conducted at the SGP-CF site, where the requisite observations exist. Section 6 considers the use of vegetation leaf area index (LAI) as an alternative coupling agent to that of soil moisture and discusses substantive differences between observed and modeled couplings with LAI at the SGP-CF site. The simulated couplings with LAI also are used to interpret the contributions to local surface evaporation of bare ground versus vegetated surfaces in the model. Finally, section 7 offers concluding remarks.

2. Observational Data

Our study investigates LAC during the warm season (May-June-July-August or MJJA) when the land-atmosphere coupling at SGP is most intense. In the vicinity of the SGP-CF ungrazed pasture (grass-covered) site, three independent measurements of shallow-depth soil moisture (SM) are available for the years 2003–2011. These SM data sets are designated by the acronyms SWATS (Soil Water and Temperature System), EBBR (Energy Balance Bowen Ratio), and CO2FLX (Carbon Dioxide Flux Measurement Systems), which may be accessed from the ARM Best Estimate: Land section of the ARM data archive (http://www.archive.arm.gov/discovery) at hourly sampling intervals (Xie et al., 2014).

The Soil Water and Temperature System (SWATS) provides vertical profiles of soil temperature and moisture (Bond, 2005; Schneider et al., 2003). The SWATS instrument imposes repeating electrical heating pulses and measures the subsequent temperature rise and decay from heat dissipation. The lower the temperature rise and the more rapid its decay, the higher is the soil moisture content, with the exact relationship depending on the local soil texture and other properties. To provide measurement redundancy, SWATS observations are taken at multiple depths in "east" and "west" profiles spaced about a meter apart (designated as SWATS-E and SWATS-W). Where both profiles of data are available, these twin hourly SM values at the CF site are averaged and treated as a single time series in our study. However, when data from one of these profiles suffer from extensive erroneous or missing values (e.g., for the west profile during the period MJJA of 2009–2011 at the CF site), only data from the alternative profile are used.

Colocated with the SWATS instrument at SGP-CF is the Energy Balance Bowen Ratio System (see fuller description below), whose chief purpose is to estimate surface latent and sensible heat fluxes (Cook, 2016a); but the EBBR instrumentation also includes an ancillary component that measures SM by five probes

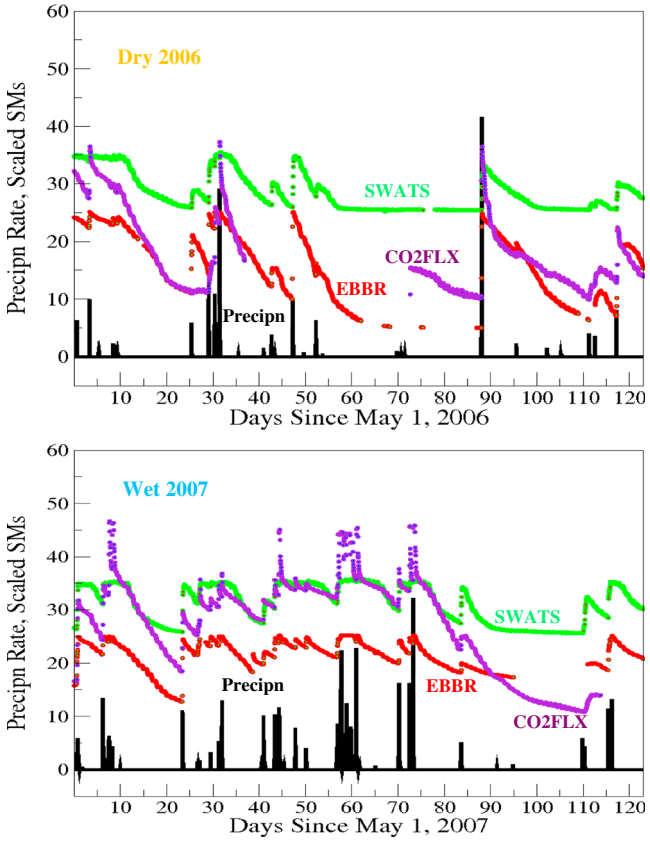

Figure 1. Time series of three independent measurements of shallow depth soil moisture SM at the SGP-CF site (coordinates 36.61°N, 97.48°W) in the (top) anomalously dry 2006 MJJA and in the (bottom) anomalously wet 2007 MJJA season. In each year, precipitation rates are shown in black, SWATS 5 cm SM in green, EBBR 2.5 cm SM in red, and CO2FLX 5 cm SM in violet. Note that the SM values (in units of m^3/m^3) are multiplied by a factor of 100, so that they can be displayed on the same scale as the precipitation rate (in units of mm h^{-1}).

that detect the moisture-sensitive dielectric constant. The SM values are derived from an average of the readings over the five sensors and are reported in gravimetric units (kg water/kg soil) that are a function of local soil properties. From knowledge of the density of the local soil with respect to water, EBBR SM values are converted to the more commonly used volumetric units (m^3/m^3).

The Carbon Dioxide Flux Measurement Systems (CO2FLX) observations of soil moisture and various atmospheric variables are conducted near the center of a wheat field immediately south of the grass-covered CF site (Fischer, 2005). Since wheat is typically harvested in June, during much of the MJJA study period this field is covered with either unharvested senescent wheat or wheat stubble that is equivalent to nonactive vegetation. Hence, the CO2FLX observations are likely to display some deviations from those at the CF site that are due solely to differences in land cover. As in the EBBR SM instrumentation, CO2FLX SM sensors include electrodes and an oscillator whose resonant frequency depends on the dielectric constant (electrical capacitance) of the soil, which is sensitive to the moisture content.

EBBR measurements of SM are only made at 2.5 cm depth. CO2FLX observations are available at both 5 cm and 15 cm depths, and SWATS measurements range from depths of 5 cm to 175 cm at some ARM stations. For our study, however, only 5 cm depth values of CO2FLX and SWATS SM are considered, for comparison with the 2.5 cm EBBR measurements.

Figure 1 compares the temporal variation of these three estimates of shallow-depth soil moisture at the CF site, and in relation to observed precipitation events, during the MJJA season of the relatively dry and wet years 2006 and 2007, respectively. The SWATS SM data vary over a reduced range of values compared to both the CO2FLX and EBBR. This is especially evident in the dry year 2006, when CO2FLX and EBBR values plunge to as low as about 0.1 m^3/m^3, while the minimum value of SWATS is only about 0.25 m^3/m^3. The anomalous minima of the SWATS SM data set result from the inability of its instrument probe to measure lower SM values than 0.25 m^3/m^3 (Cook & Kyrouac, 2015). This is because the probe's electrical signal has difficulty penetrating soils with substantial clay content (as at the CF site) when soil moisture is low, making the calibration of the SWATS instrument problematic. (This limitation also exists for SWATS SM measurements made at lower depths at the CF site.)

On the other hand, there are substantially fewer missing values in the SWATS measurements than in the CO2FLX and EBBR SM data. Together with missing surface atmospheric observations, this substantially reduced the number of available soil moisture-atmospheric pairings to investigate. For a total of 1,107 days in the MJJA 2003–2011 study period, for example, there are an average of 1,076 daily soil moisture-atmospheric covariance pairs for SWATS, 875 for CO2FLX, and 822 for EBBR soil moisture measurements.

For our study, the available ARM atmospheric measurements of interest are surface air temperature *T*, relative humidity RH, and latent and sensible heat fluxes *L* and *H*. At the CF site, the ARM Best Estimate (ARMBE) archives were used as a primary source of data for these variables (Phillips & Klein, 2014; Xie et al., 2010), but alternative measurements also were employed where available. For example, at the CF site the ARMBE surface temperature and humidity are measured by Surface Meteorological (SMET) probe transmitters (Ritsche, 2008), while alternative temperature and humidity measurements also are recorded by the CO2FLX instrument system (Fischer, 2005) that is located in the harvested wheat field just south of the CF site.

At the grass-covered CF site, the ARMBE surface turbulent fluxes are estimated by the EBBR instrumentation system (Cook, 2016a). Flux estimates are derived from measurements of surface net radiation, ground heat flux, and the vertical gradients of temperature and relative humidity that are made by a net radiometer,

temperature/relative humidity and soil temperature/moisture/heat flow probes, and a wind speed sensor. The meteorological data are used to calculate bulk aerodynamic (BA) fluxes for producing a value-added product known as BAEBBR. This is a best estimate of the turbulent fluxes that corrects sunrise/sunset spikes occurring in the raw EBBR fluxes, when the temperature and relative humidity gradients are of opposite sign and nearly equal in magnitude. The EBBR soil moisture at 2.5 cm depth also is used in order to calculate the soil heat conductivity, for correction of the soil heat flow plate measurements. Together with the temporal change in soil temperature measurements, this calculated conductivity provides an estimate of the ground heat flux, which impacts the magnitudes of the turbulent fluxes.

Eddy correlation (ECOR) sonic anemometers and H_2O/CO_2 analyzers provide alternative measurements of surface sensible and latent heat fluxes that are estimated directly from the correlation of vertical velocity with air temperature and water vapor density, respectively (Cook, 2016b). Over the same surface, ECOR sensible and latent heat flux measurements are generally of smaller magnitude than those of the EBBR instrument, since the latter are forced to be equal to the local available energy. The ECOR instrument near SGP-CF is sited close to the boundary between the grass-covered CF site and the harvested wheat field to the south. ECOR measurements thus are influenced by both surface types (depending on wind direction) and so will also differ from the EBBR measurements on the grass-covered CF site. Another difference is that the ECOR data near SGP-CF are available for one fewer warm season (MJJA of 2004–2011) than the EBBR (MJJA of 2003–2011).

3. Analysis Approach, Metrics, and Observational LAC Results

To analyze the terrestrial component of LAC—whether in observations or model simulations—we adopt the approach of Betts (2004, 2009) and focus on covariance relationships between *daily averages* of soil moisture and surface atmospheric variables such as the turbulent fluxes, relative humidity, and temperature. The daily average quantities are built up from hourly, or in some cases half-hourly samples, while accounting for data gaps during the MJJA warm seasons of 2003–2011 (see Phillips & Klein, 2014 for details).

The covariance relationships are displayed as scatterplots, with daily averages of soil moisture and of a specified atmospheric variable oriented along the x axis and y axis, respectively. A quantitative measure of the coherence of an x-y scatterplot is provided by the correlation coefficient R:

$$R = \mathrm{cov}(x,y)/(\sigma_x\sigma_y) = < x'y' > /(\sigma_x\sigma_y)$$

consisting of the temporal sum (denoted by $< >$) of the product of daily departures x' and y' of each variable from its multiyear statistical mean value, where σ_x and σ_y are the corresponding standard deviations. It may also be advisable to filter out the influence of the seasonal cycle (e.g., by subtracting the multiyear climatology from each month's "raw data") before computing R. However, other SGP studies of this type (e.g., Williams & Torn 2015), imply that the impact of the seasonal cycle on LAC metrics is of second-order importance for this region.

Because R may be sensitive to mismatches in the standard deviations of the x and y variables (i.e., large variability σ_y with small variability σ_x, or vice versa), Dirmeyer (2011) recommends use of a "sensitivity index" I:

$$I = \sigma_x\, b$$

where $b = \mathrm{cov}(x,y)/\sigma_x^2$ is the slope of the least squares regression line $y = a + bx$ calculated from the scatter of y versus x. Index I thus measures the magnitude of the average variation in y for a one-sigma variation in x and takes on the same units as the y variable. It also can be seen that $I = \sigma_y R$, so that I and R are related through the scaling coefficient σ_y. We therefore employ I as an auxiliary LAC metric to R.

To assess the statistical significance of R, the number of statistically independent daily average samples of y versus x must be estimated. Accounting for data gaps, there are a minimum of about 822 x-y paired samples in the 2003–2011 MJJA records associated with the EBBR soil moisture data, which suffer the most data gaps; but because these samples are serially correlated, they are not all statistically independent. We attempted to estimate an upper bound for the serial correlation interval by analyzing the e-folding length of the autocorrelation function of the slowly varying SWATS data in seasons where data gaps were not an issue. From this limited analysis, we conservatively estimated that only every fifth daily average was statistically independent (see also Dirmeyer et al., 2012). Under this assumption, the EBBR SM data set contains about 164 such

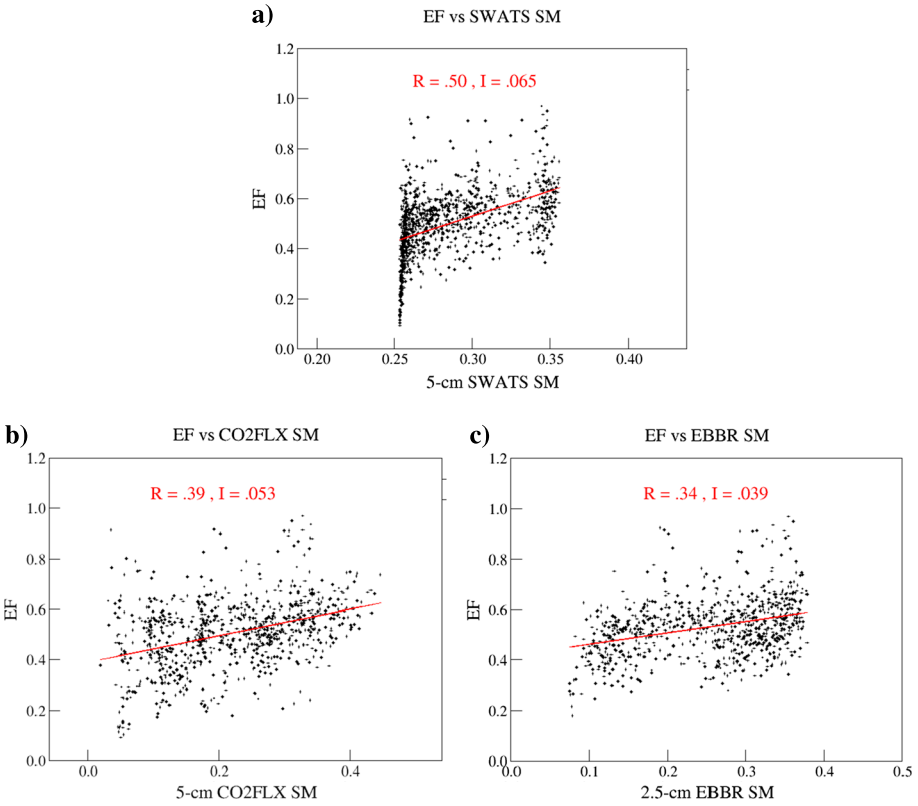

Figure 2. The 2003–2011 MJJA daily average scatter of evaporative fraction EF, measured by the EBBR instrument, versus (a) SWATS 5 cm depth soil moisture, (b) CO2FLX 5 cm depth soil moisture, and (c) EBBR 2.5 cm depth soil moisture, all observed at the SGP-CF site. SM values are in volumetric units of m^3/m^3, and EF is dimensionless. The coupling-strength metrics *R* and *I* are also shown in each case (consult section 3 of the text for details).

samples. Applying a one-tailed Student's *t* test (e.g., Bulmer, 1979) that assumes physically based foreknowledge of the sign of the correlation indicates that $|R| > 0.18$ is statistically significant with probability $p = 0.01$ (i.e., a 99% confidence level). Where *R* is statistically significant, *I* is also assumed to be so, since it scales with *R*.

3.1. Observational Estimates of LAC at the SGP-CF Site

The coupling between soil moisture and surface evaporation is central to the terrestrial component of LAC; but this coupling is better expressed by the covariance between SM and the evaporative fraction EF, which is a quasi-conserved quantity on daily time scales (Gentine et al., 2011; Shuttleworth et al., 1989). For measured values of surface latent heating *L* and sensible heating *H*

$$\mathrm{EF} = L/(L+H)$$

EF can be calculated from BAEBBR value-added estimates of *L* and *H*. Illustrative scatterplots of daily averages of EF with each of the independent shallow-depth SM measurements at CF (SWATS, CO2FLX, and EBBR) are shown in Figure 2. EF is seen to covary positively with all three SM measurements, and the LAC strength metric *R* ranges from a low value of 0.37 for the 2.5 cm depth EBBR SM to a high value of 0.50 for the 5 cm depth SWATS, with the 5 cm depth CO2FLX SM measurements yielding an intermediate value of 0.39. The coupling metric *I* is similarly ordered, with a low value of 0.042 displayed by the EBBR SM, 0.053 by CO2FLX, and 0.065 by SWATS. (A corresponding disparity occurs when comparing LAC estimated from SWATS versus CO2FLX SM, both at 15 cm depths).

Qualitatively similar covariance scatter is exhibited by the surface relative humidity RH (measured by the SMET system—see above description) versus the three SM measurements (Figure 3). The LAC metrics for

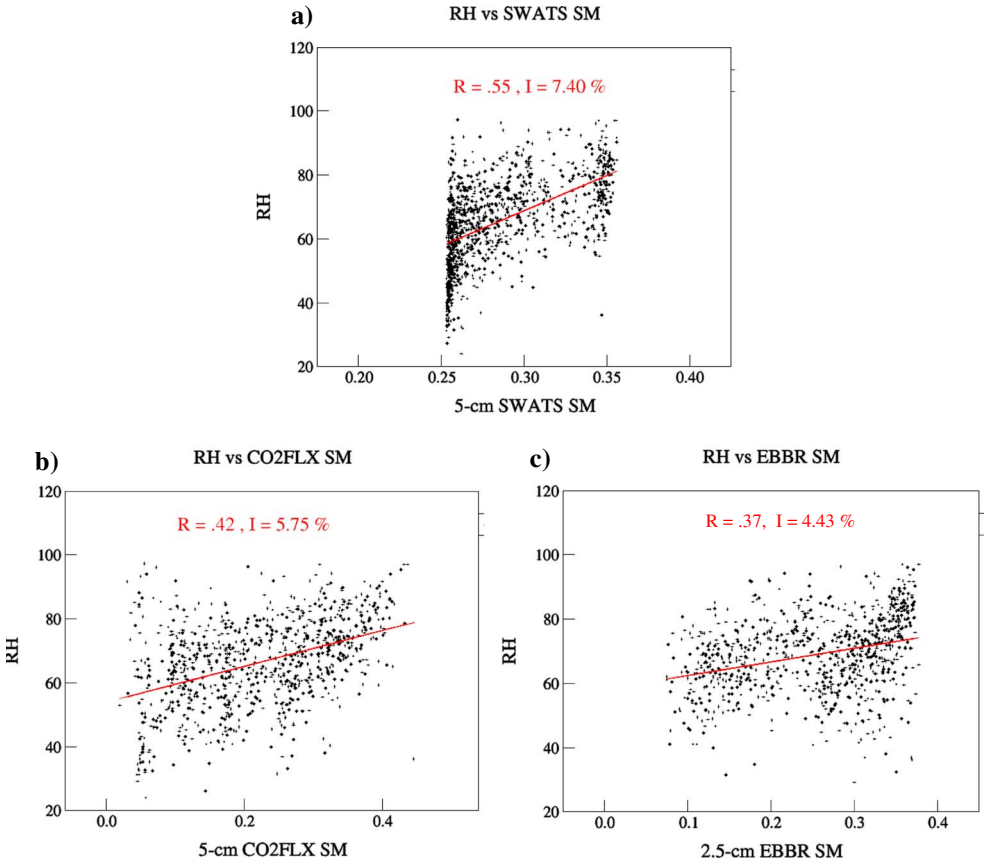

Figure 3. As in Figure 2 except for the daily average scatter of surface relative humidity RH (in %) plotted versus shallow-depth soil moisture (in m^3/m^3) given by (a) SWATS, (b) CO2FLX, and (c) EBBR measurements, respectively.

RH also are ordered similar to those for EF: the strongest coupling with RH is shown by SWATS SM ($R = 0.55$, $I = 7.40\%$) and the weakest by EBBR ($R = 0.37$, $I = 4.43\%$), with CO2FLX SM displaying intermediate coupling strength ($R = 0.42$, $I = 5.75\%$).

In contrast to EF and RH, surface air temperature T (also measured by the SMET system) exhibits a negative covariation with soil moisture (Figure 4). The magnitude of LAC strength for SM-T coupling, as measured by the absolute value of the correlation coefficient R, is lower than for SM-EF or SM-RH couplings; but once again, the coupling of T with SWATS SM displays the most negative magnitudes of R and I (-0.36 and -1.73 K, respectively), followed by CO2FLX ($R = -0.32$, $I = -1.54$ K) and EBBR SM ($R = -0.27$, $I = -1.24$ K).

The available 2003–2011 record length of warm-season observations was assumed sufficient for estimation of SM and LAC statistics of acceptable accuracy (Findell et al., 2015; Ford et al., 2016). Analysis of the variations in R and I values for SM-EF coupling that occur with the progressive inclusion of each year's warm season (Table S1) raises some caveats, however. In general, the estimated values of R and I coupling metrics associated with the three independent SM measurements appear to "stabilize" after the inclusion of about seven warm seasons (2003–2009). However, including data for the last 2 years—the very wet 2010 warm season and the very dry 2011—disrupts the relative stability of R and I attained for years 2003–2009, shifting their values by an average of several percent for correlations associated with SWATS SM, but by more than 10% for CO2FLX and EBBR SM. Thus, for 9 years of warm-season measurements, the inclusion of data from a few exceptional years can alter the overall estimates of R and I to a surprisingly large degree for some SM measurements.

The consistently high LAC strength metrics for SWATS SM measurements, compared to those for CO2FLX or EBBR, also warrant further analysis. First, from comparison of Figures 2–4, the overall range of soil moisture values in daily average 5 cm SWATS data at SGP-CF is substantially less than what is found in either the CO2FLX or EBBR data. For instance, the minimum value of SWATS SM is about 0.25 m^3/m^3 (a consequence

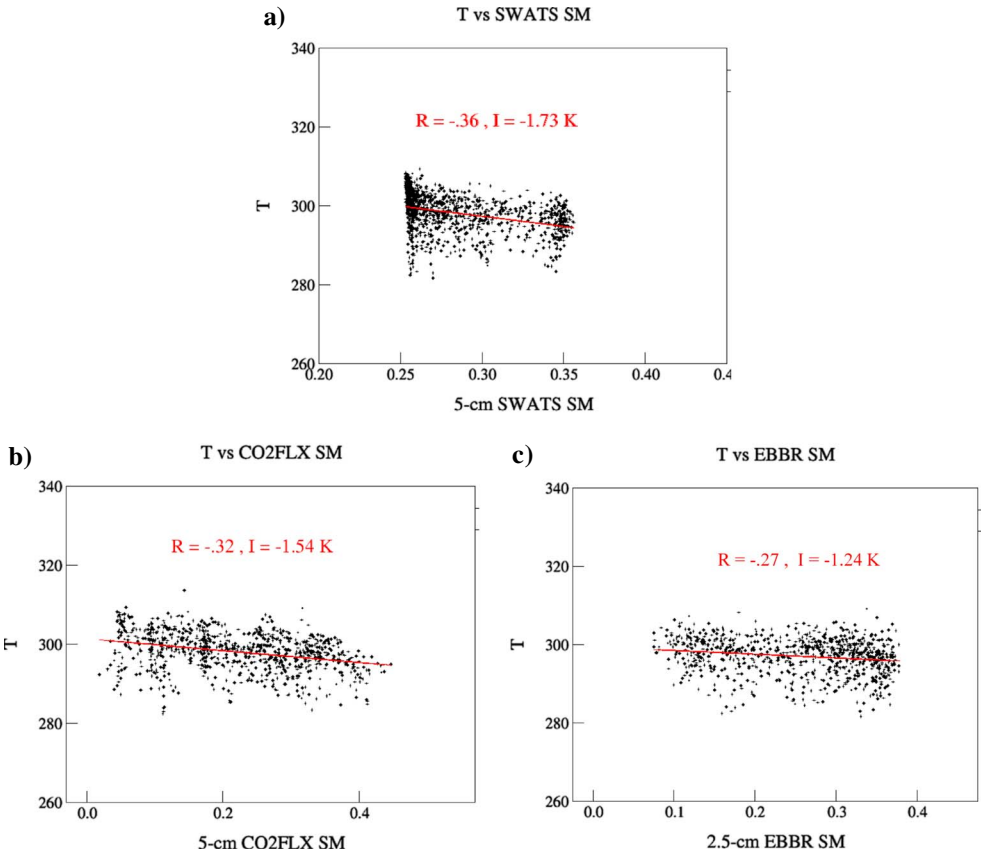

Figure 4. As in Figure 2 except for the scatter of daily average surface air temperature *T* (in K) plotted versus shallow-depth soil moisture given by the (a) SWATS, (b) CO2FLX, and (c) EBBR measurements, respectively.

of the SWATS instrumental limitation mentioned in section 2), which is much less dry than the lowest values seen in the other SM data sets that lie below 0.1 m^3/m^3. It is therefore possible that the covariation of relatively low values of EF, RH, and *T* with an artificially high minimum SWATS SM may skew the slopes of the respective regression lines higher, resulting in overestimation of the LAC strength metrics.

We investigated the effects of imposing the same reduced range on the CO2FLX and EBBR SM data when calculating their LAC metrics; but in following this protocol we found that *R* and *I* for the non-SWATS data could not be raised substantially toward the corresponding higher SWATS values. To cite one example, the covariation of *T* with EBBR SM restricted to values greater than 0.25 m^3/m^3 yielded LAC strength metrics $R = -0.30$ and $I = -1.35.92$ K, which are only moderately different than the metrics obtained from the covariation of *T* with the unrestricted EBBR SM ($R = -0.27$, $I = -1.24$ K).

We also considered the possibility that the lower values of *R* and *I* metrics in the CO2FLX data set might be explained by sampling errors in the CO2FLX or EBBR measurements, which display many more data gaps than the SWATS. To test this hypothesis, the SWATS data were degraded by eliminating daily average values of SM on those days where CO2FLX or EBBR measurements showed missing data. Then the LAC strength metrics for the SM-EF, SM-RH, and SM-T couplings were recalculated (see Table 1). While the EBBR-sampled SWATS data produced LAC strength metrics *R* and *I* that were somewhat lower than the original SWATS data set, the metrics calculated from the CO2FLX-sampled SWATS data were almost the same magnitude. Variations in sample size among the three SM data sets thus are not sufficient to explain the different magnitudes of the associated LAC strength metrics. These instead appear to be due to differences in instrumentation, land cover, and depth of SM measurement.

The LAC metrics shown in Figures 2–4 reflect only differences in SM measurements. In order to test the impacts of alternative measurements of the atmospheric variables on the LAC metrics, latent and sensible heat fluxes recorded by the ECOR instrument (displaying the influence of both grass-covered and wheat-covered

Table 1
For the SGP-CF Site, Correlation R *and Sensitivity Index* I *of the Atmospheric Surface Evaporative Fraction EF (Estimated From BAEBBR Measurements of the Turbulent Fluxes), Relative Humidity RH, and Air Temperature* T*, With Respect to the SWATS SM Data*

Soil moisture measurement	EF	RH	T
SWATS	R = .50 [0.39 to 0.60] I = 0.065	R = 0.55 [0.45 to 0.64] I = 7.40%	R = − 0.36 [−0.24 to −0.47] I = −1.73 K
CO2FLX-sampled SWATS	R = 0.52 I = 0.070	R = 0.54 I = 7.32%	R = −0.38 I = −1.82 K
EBBR-sampled SWATS	R = 0.42 I = 0.049	R = 0.47 I = 5.52%	R = −0.22 I = −1.00 K
CO2FLX	R = 0.39 [0.25 to 0.51] I = 0.053	R = 0.42 [0.29 to 0.54] I = 5.75%	R = −0.32 [−0.18 to −0.45] I = −1.54 K
EBBR	R = 0.37 [0.23 to 0.50] I = 0.042	R = 0.37 [0.23 to 0.50] I = 4.43%	R = −0.27 [−0.12 to −0.41] I = −1.24 K

Note. R and I values also are shown for SWATS data that are reduced according to available CO2FLX and EBBR soil moisture samples for the MJJA warm seasons in 2003–2011. Also listed are the R and I values of EF, RH, and T associated with the CO2FLX and the EBBR soil moisture data. The most extreme positive or negative value of the correlation for each atmospheric variable is shown in red and the least extreme value in blue. In addition, the range of ±95% confidence levels for the R values associated with the SWATS, CO2FLX, and EBBR soil moisture measurements is shown in brackets (assuming 215, 175, and 164 are statistically independent pairs of atmospheric and soil moisture variables, respectively, see section 3.1 discussion).

surfaces) were substituted for the grass-covered EBBR measurements. Observations of RH and T by the CO2FLX instruments on the wheat-covered surface also were substituted for their SMET equivalents on the grass-covered CF site. The impacts of these atmospheric-measurement substitutions on the LAC metrical values are listed in Table 2, together with the R and I values shown in Figures 2–4. Only modest differences in estimated LAC strengths (generally, more in I than in R) are seen to result from such alternative atmospheric measurements, while the impacts of the different choices of SM measurement are generally greater.

Of course, there is also an inherent statistical uncertainty in the estimated R value of an atmospheric variable correlated with a particular soil moisture data set; but the probability distribution of R becomes progressively more skewed as its sampled mean value increases, making the estimation of confidence limits on R problematical. Instead, R can be transformed into a normal variate Z:

$$Z = 0.5^{*} \ln [(1 + R)/(1 - R)]$$

with standard error $\sigma_Z = 1/(n - 3)^{1/2}$, where n is the number of statistically independent pairs of soil versus atmospheric observations (Fisher, 1921). The $\pm 2\sigma_R$ (±95%) confidence levels for R then can be obtained by an inverse transformation of the corresponding $Z \pm 2\sigma_Z$ values (e.g., Snedecor & Cochran, 1967). (When R is negative, as for the SM-T correlation, the absolute value of R is used to obtain Z, and the negative sign is restored after completing the inverse transformation.)

Estimates of the range of the ±95% confidence limits for R values associated with SWATS, CO2FLX, and EBBR soil moistures (assuming 215, 175, and 164 statistically independent pairings, respectively) are listed in

Table 2
The 2003–2011 Warm-Season (MJJA) Correlations R *and Sensitivity Coefficients* I *of the SWATS, EBBR, and CO2FLX Shallow-Depth Soil Moisture Content Measurements With Respect to Observationally Based Estimates of Surface Evaporative Fraction EF, and Surface Relative Humidity RH and Temperature* T*, All in the Vicinity of the SGP-CF Site (Coordinates 36.61°N, 97.48°W)*

	EF		RH		T_s	
Soil moisture data sets	BAEBBR	ECOR	SMET	CO2FLX	SMET	CO2FLX
SWATS	R = 0.50 I = 0.065	R = 0.54 I = 0.083	R = 0.55 I = 7.40%	R = 0.51 I = 6.52%	R = −0.36 I = −1.73 K	R = −0.37 I = −1.80 K
CO2FLX	R = 0.39 I = 0.053	R = 0.40 I = 0.061	R = 0.42 I = 5.75%	R = 0.44 I = 5.58%	R = −0.32 I = −1.54 K	R = −0.30 I = −1.46 K
EBBR	R = 0.37 I = 0.042	R = 0.47 I = 0.064	R = 0.37 I = 4.43%	R = 0.38 I = 4.43%	R = −0.27 I = −1.24 K	R = −0.26 I = −1.19 K

Note. Here EF is derived from surface latent and sensible heat fluxes that are measured by the BAEBBR system or, alternatively, by the ECOR instrument that is part of the CO2FLX system located in a wheat-covered field adjacent to the CF site. The RH and T values are ARM best estimate (ARMBE) data obtained from the ARM surface meteorology observation system (SMET) instruments or from CO2FLX tower measurements. Note that the ECOR data are available only for the years 2004–2011, while all others are for the period 2003–2011.

Table 3
Selected Extended Facility Geographical Location, Dominant Soil and Vegetation Types, and Distance From the CF

Site	Location soil and vegetation type	Distance to CF (km)	IDW	*R*, *I* SWATS	*R*, *I* EBBR
E4	Plevna, KS (38.0°N, 98.3°W) fine sandy loam, shrubs/grass	157.44	0.101	0.55 [0.42 to 0.66], 0.062	0.50 [0.37 to 0.61], 0.058
E7	Elk Falls, KS (37.4°N, 96.2°W) silt loam, pasture	143.00	0.111	0.38 [0.23 to 0.51], 0.038	0.22 [0.07 to 0.36], 0.022
E9	Ashton, KS (37.1°N, 97.2°W) loam, pasture	53.05	0.306	0.21 [0.05 to 0.36], 0.022	0.15 [−0.01 to 0.30], 0.017
E12	Pawhuska, OK (36.7°N, 96.3°W) sandy loam, tallgrass prairie	108.88	0.146	0.090 [−0.08 to 0.25], .008	0.14 [−0.01 to 0.29], 0.012
E15	Ringwood, OK (36.4°N, 98.2°W) sandy loam, pasture	70.68	0.225	0.33 [.17 to 0.47], 0.033	0.28 [0.13 to 0.42], 0.032
E20	Meeker, OK (35.5°N, 96.9°W) fine sandy loam, pasture	144.64	0.110	0.52 [0.39 to 0.63], 0.059	0.57 [0.46 to 0.67], 0.064
Regional average values: R = 0.35 [0.20 to 0.49], I = 0.037 (or R = 0.31 [0.16 to 0.44], I = 0.032) for SWATS SM R = 0.31 [0.15 to 0.45], I = 0.034 (or R = 0.27 [0.12 to 0.41], I = 0.030) for EBBR SM.					

Note. Also listed are the local coupling strength metrics R and I determined from the scatter of evaporative fraction EF (BAEBBR measurement) relative to soil moisture SM (both SWATS and EBBR measurements). In addition, the inverse-distance weightings (IDW) relative to the CF are shown for each station. Finally, the last row lists the regional averages of the unweighted and weighted (in parentheses) R and I values across all the extended facility sites. In addition, for each R value the range of the estimated ±95% confidence limits also is given in brackets, assuming 148 independent samples for SWATS-EF and 168 for EBBR-EF correlations.

brackets in Table 1. The estimated ±95% confidence intervals for each of the measured correlations R in Figures 2–4 are all found to overlap for the three different SM measurements, whether correlated with EF, RH, or T. For instance, in the case of SM-EF covariations (shown in Figure 2), the +95% confidence limits for EF correlated with EBBR and CO2FLX soil moistures are 0.50 and 0.51, respectively, which exceed the −95% confidence limit of 0.39 for SWATS soil moisture (Table 1). Thus, from a purely statistical standpoint, correlations of the selected atmospheric variables with the three different soil moisture measurements cannot be distinguished from one another, at a 95% level of confidence.

3.2. Observational LAC Estimated Over the SGP Region

Results reported in the last section imply substantial uncertainties in observed LAC strengths at the SGP-CF site. It should be possible to obtain a more statistically robust estimate of LAC by considering SM-EF covariation across the SGP region. Such a regionally representative estimate of LAC also should make a more suitable benchmark for evaluating coupling strength in CAM5.1/CLM4 model simulations that are realized on a 0.9 × 1.25° horizontal grid. This section illustrates how such a regionally aggregated estimate of SM-EF coupling strength, central to the terrestrial component of LAC, can be obtained.

While some two dozen ARM extended (E) facilities surround the CF site, there are only six where both soil moisture and atmospheric surface variables were recorded continuously over the MJJA 2003–2011 study period. Their geographic locations and soil/vegetation types are listed in Table 3. Available soil moisture observations at these E facilities include half-hourly to hourly measurements of 2.5 cm EBBR and 5 cm SWATS soil moisture. Compared to the CF site, more SM data are missing for both the SWATS east and west soil profiles (SWATS-E and SWATS-W). Hence, instead of averaging profile values, it is necessary to choose SM values from one or the other profile, depending on which includes the more complete data time series. However, an advantage of the SWATS soil moisture measurements at the E sites is that they extend over a moisture range comparable to that of the EBBR measurements, owing to soils that contain less clay than at the CF site (see section 2 discussion and Table 3). At these E sites surface latent and sensible heat flux measurements, from which estimates of evaporative fraction EF can be derived, are provided by BAEBBR value-added products. On average, for the MJJA 2003–2011 study period, there are 740 SWATS SM-EF sample pairs at the selected E sites and about 840 EBBR SM-EF pairs, yielding statistically independent sample sizes of about 148 versus 168, respectively.

In their detailed analysis of in situ observations of soil moisture over the conterminous U.S., Dirmeyer et al. (2016) found that the temporal variability of soil moisture was less sensitive to aggregation over neighboring sites than was the temporal mean. For estimating a regional average of SM-EF coupling strength, it thus seems advisable to spatially average a collection of locally calculated SM-EF values of R and I, rather than to compute these metrics from the scatter of SM and EF data that are spatially averaged. In fact, LAC metrics across the six E facilities display much spatial heterogeneity, exemplified by Figure S1 in the supporting information that contrasts SM-EF daily average scatterplots (employing both SWATS and EBBR SM versus EBBR EF data) at sites E4 (Plevna, Kansas) and E12 (Pawhuska, Oklahoma). Despite quantitative differences in coupling

estimates for SWATS versus EBBR SM, LAC strength metrics are consistently much higher at the E4 site (R = 0.55, I = 0.062 for SWATS; R = 0.50, I = 0.058 for EBBR SM) than at E12 (R = 0.09, I = 0.008 for SWATS; R = 0.14, I = 0.012 for EBBR SM), where the LAC strength metrics are so low that their statistical significance is questionable (see section 3.1 discussion).

The range of SM values at site E4 (ranging between about 0.08 and 0.20 m^3/m^3; Figures S1a and S1b) versus those at E12 (ranging between about 0.21 and 0.40 m^3/m^3; Figures S1c and S1d) reflects a well-known west-east (eastward increasing) precipitation gradient across the SGP region (Sisterson et al., 2016). Because E4 experiences more moisture stress than E12, soil moisture should generally exert greater control on warm-season EF at E4 (Ford, Rapp, Quiring, Blake, 2015; Nicholson, 2015; Phillips & Klein, 2014), thus accounting for the observed stronger coupling at E4. However, when considering the local LAC metrics across all six extended facility sites, such an explanation seems too simplistic. For example, although average local soil moisture values at sites E7, E9, E12, and E20 are all about 0.3 m^3/m^3, their LAC metrics differ substantially (Table 3). This outcome implies that diverse local soil and land cover types (Table 3, column 2) also strongly impact LAC strength across the SGP region. It suggests as well that the available observations of shallow soil moisture are not very indicative of the impact that vegetation, rooted at deeper soil depths, can have on EF.

Columns 5 and 6 of Table 3 list the SM-EF strength metrics R and I for SWATS versus EBBR soil moisture, along with the range of estimated ±95% confidence levels. At each site, the confidence intervals of SWATS-associated correlations overlap the EBBR-associated ones, implying that the respective site-specific R values are statistically indistinguishable. However, the very low SWATS- and EBBR-associated correlations at sites E9 and E12 can be distinguished, with 95% confidence, from the highest correlations at sites E4 and E20. For E9 this may be the result of the soil texture (loam), whereas for E12 it is likely influenced by the vegetation (prairie tallgrass), whose roots extend to much greater depths than the pasture grass at the other locations. Tallgrass plants draw most of their moisture from well below the 0–5 cm top layer of soil and thus are less dependent than pasture grass on the shallow-layer SM.

Listed just below Table 3 are the cross-site regional averages of R and I for SWATS (R = 0.35, I = 0.037) and EBBR (R = 0.31, I = 0.034) soil moistures, respectively, where these regional estimates are calculated from a simple linear averaging of R and I over the six E sites. In addition, an inverse-distance-weighting algorithm, centered on the CF site, is used to compute an alternative regional average of each LAC strength metric $< M >$:

$$< M >= \Sigma_i \, (w_i \, M_i)/\Sigma_i \, w_i, \text{where weight } w_i = 1/D_i/D_i$$

Here M_i is a strength metric R or I at an extended site E_i located at distance D_i from the CF site. D_i and the associated inverse-distance weights for each E site all are listed in Table 3. The corresponding weighted regional averages (i.e., summations of the weighted R and I values) are shown in parentheses at the bottom of columns 6 and 8 for SWATS (R = 0.31, I = 0.032) and EBBR (R = 0.27, I = 0.030), respectively. Weighted and unweighted regional average values of R and I thus do not differ much from one another, and they also are rather insensitive to the choice of SM data set: the regional average R value lies between 0.27 and 0.35 (the corresponding I value between 0.030 and 0.037), which are indistinguishable with 95% confidence. These regional-average estimates of R and I provide observational benchmarks for evaluation of model simulations of SM-EF coupling strengths, to be taken up in following sections.

4. Model Properties and Simulation Configurations

The CAM5.1 atmospheric model (Neale et al., 2012) operates on a horizontal grid with resolution 0.9 × 1.25° latitude/longitude and on a vertical grid of 30 levels. Its physical parameterizations include the radiative transfer scheme of Iacono et al. (2008); shallow and deep convective parameterizations after Park and Bretherton (2009), Zhang and McFarlane (1995), and Neale et al. (2008); a planetary boundary layer and associated moist turbulence scheme developed by Bretherton and Park (2009); prognostic cloud physics and microphysics schemes of Morrison and Gettelman (2008), Gettelman et al. (2010), and Park et al. (2014); and a prognostic aerosol scheme after Liu et al. (2012).

The CLM4 land model (Oleson et al., 2010) uses the same horizontal grid as the atmospheric model, includes 15 vertical soil layers and 5 snow layers, and accounts for heterogeneity in surface types (glacier, lake, wetland, etc.). The CLM4 represents vegetated surfaces by as many as 16 plant functional types (PFTs). In

our simulations, a version of CLM4 *without* dynamic vegetation or carbon fluxes was employed, and distinct vegetation properties such as PFT fractions and canopy top and bottom heights instead were prescribed for each grid box. Leaf and stem area indices (LAI and SAI) were similarly prescribed but varied temporally according to monthly climatologies.

Surface radiative fluxes account for vegetation and canopy properties, and turbulent fluxes follow Monin-Obukhov similarity theory, as formulated by Zeng et al. (1998). Depth-dependent moisture storage in CLM4 is the net outcome of parameterized precipitation infiltration, surface and subsurface runoff, diffusion of soil water, subcolumn drainage, and interactions with groundwater, as described by Zeng and Decker (2009).

We investigated simulations in which the CAM5.1/CLM4 coupled system was run in two qualitatively different configurations: free-running Atmospheric Model Intercomparison Project (AMIP) and controlled hindcast (HC) simulations, both over the period 1997 to 2012. In the AMIP simulation, observed sea surface temperatures (SSTs) and sea ice extents (SIEs) were prescribed as ocean boundary conditions. The atmospheric and land states both were initialized from a model climatology determined after a prior long spin-up of soil moisture. For the controlled HC configuration, the SSTs and SIEs also were prescribed as in the AMIP experiment, but the three-dimensional fields of atmospheric prognostic dynamic and thermodynamic state variables instead were initialized at the beginning of each simulation day according to their ERA-Interim Reanalysis values. Initialization of prognostic aerosol concentrations proceeded by nudging the atmospheric U and V winds, using a Newtonian relaxation method, toward their ERA-Interim values. (Nudging only the model winds resulted in more realistic aerosol concentrations than when the model atmospheric temperature and humidity were also nudged toward ERA-Interim values.) The daily initial conditions for the land state were determined by running the CLM4 in an offline configuration, where it was forced with observed winds, precipitation, and downward shortwave and longwave surface radiative fluxes. This land initialization procedure yielded more realistic values of soil moisture than in the free-running AMIP simulation.

For each day's initialization of atmosphere and land, hindcasts (i.e., model forecasts of historical weather conditions) were generated over the following 3 days, with a steadily increasing drift of the model hindcasts from observations. Since day 1 hindcasts often show spurious perturbations resulting from initialization "shock"; LAC results for day 2 hindcasts were analyzed in our study (see Ma et al., 2015 for further details).

5. Evaluation of Model LAC: Free-Running Versus Controlled Configurations

Similarities and differences in LAC displayed by the model in its free-running AMIP versus controlled HC configurations, as well as comparisons with the observed estimates of LAC at both the CF site and across the SGP region, are discussed next.

5.1. Model Evaluation Near the SGP-CF Site

In this section, all reported model results are those simulated at the grid point (with coordinates 36.28°N, 97.50°W) that lies nearest to the SGP-CF site (at 36.61°N, 97.48°W). Scatterplots of the covariances of coupled CAM5.1/CLM4 daily averages of EF, RH, and T with respect to 5 cm depth soil moisture are shown in Figure 5 for the AMIP simulation. LAC strength metrics R and I for the respective AMIP-simulated couplings are seen to lie well above the highest observational LAC estimates at the CF site, which are associated with the SWATS soil moisture measurements (Figures 2–4). The model exceedance of the observed strength metrics is especially dramatic for the SM-T coupling, where AMIP values $R = -0.80$ and $I = -4.45$ K are more than twice as large as the highest SM-T observational estimates ($R = -0.36$, $I = -1.73$ K, Figure 4).

Figure 6 shows the corresponding scatterplots for the controlled HC simulation. The scatter of EF versus SM (Figure 6a) displays a "kink" at an SM value of about 0.3 m^3/m^3, which is somewhat more pronounced than in the AMIP simulation (Figure 5a). Further investigation of the scatter of EF associated with evaporation from bare ground versus vegetated fractions of this model grid cell implies that this feature results from an abrupt leveling off in the variation of bare-ground EF for SM values greater than about 0.3 m^3/m^3. The clear signature of bare-ground evaporation in Figure 6a suggests that it is a strong contributor to the total EF in this model grid cell. As is found for the AMIP simulation (Figure 5), the LAC strength metrics for HC lie well above the highest observational estimates associated with the SWATS soil moisture data (Figures 2–4). The SM-EF and SM-RH coupling strengths for the HC simulation are slightly less than those for the AMIP run (compare

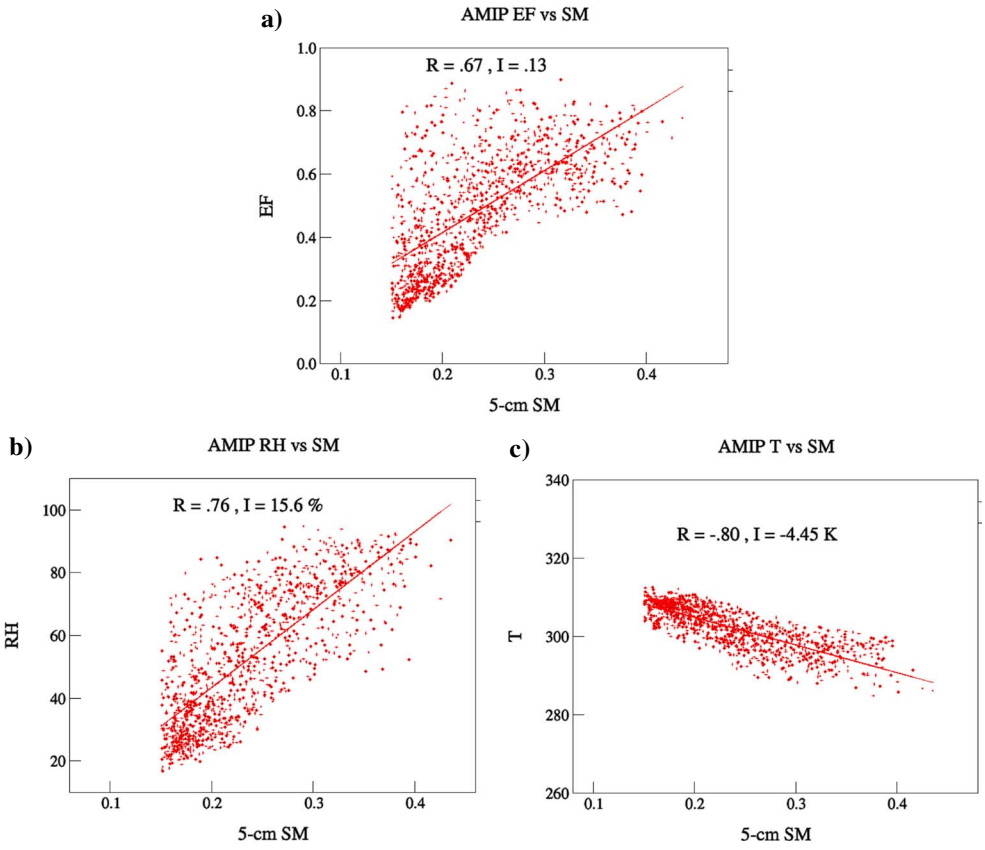

Figure 5. The 2003–2011 MJJA daily average scatter of CAM5.1 surface atmospheric variables versus CLM4 soil moisture at 5 cm depth (in volumetric units of m^3/m^3) from the free-running AMIP simulation are shown. (a) The surface evaporative fraction EF versus model SM is displayed. (b) The model surface relative humidity RH (in %) and (c) surface air temperature *T* (in K), both versus the model SM, are shown. LAC strength metrics *R* and *I* are also displayed in each case.

Figure 5a/6a and Figure 5b/6b), but the SM-T coupling strength for the HC is markedly less ($R = -0.53$, $I = -2.50$ K) than that for AMIP ($R = -0.80$, $I = -4.5$ K).

The very tight SM-T coupling in the AMIP simulation relative that for the HC (Figure 5c/6c) apparently results from the free-running model's more frequent "visits" to drier soil moisture states than in the controlled HC simulation. For instance, we can identify the "dry" portion of the model's SM-EF transition zone (between completely wilted and fully saturated SM conditions) with SM values less than ~0.25 m^3/m^3, and the "wet" portion with SM values greater than ~ 0.35 m^3/m^3. Then about 64% of SM values for the AMIP configuration are found to occur at dry levels, while only about 6% rise to wet levels; for the controlled HC configuration, however, the dry and wet SM frequencies are instead 34 and 19%, respectively.

When soil moisture in semiarid regions such as the SGP falls into drier states, its coupling with surface atmospheric variables tends to increase (Ford, Rapp, Quiring, Blake, 2015; Nicholson, 2015; Phillips & Klein, 2014). Meanwhile, surface EF falls, while surface sensible heat flux H and temperature *T* rise. The enhanced SM-T coupling for drier SM states in the free-running AMIP configuration tends to amplify a continental warm bias that is present in simulations of the CAM5.1/CLM4, as well as in many other current-generation GCMs (e.g., Klein et al., 2006; Cheruy et al., 2014; Van Weverberg et al., 2015; Merrifield & Xie, 2016). In the controlled HC configuration, however, soil moisture is prevented from falling as frequently into drier states because the land model is initialized each day by forcing it with observed precipitation. Hence, the SM-T coupling is less intense in the HC simulation than in the free-running AMIP.

Figure 7 compares time series of daily average precipitation rate *P* near the CF site in both AMIP and HC simulations with CF-observed values in the MJJA warm season of the relatively dry/wet years 2006/2007. Observed MJJA precipitation is seen to occur in sharp spikes with maximum amplitude about 80 mm d^{-1}; but precipitation events in the AMIP simulation remain mostly below 10 mm d^{-1} intensity. As would be

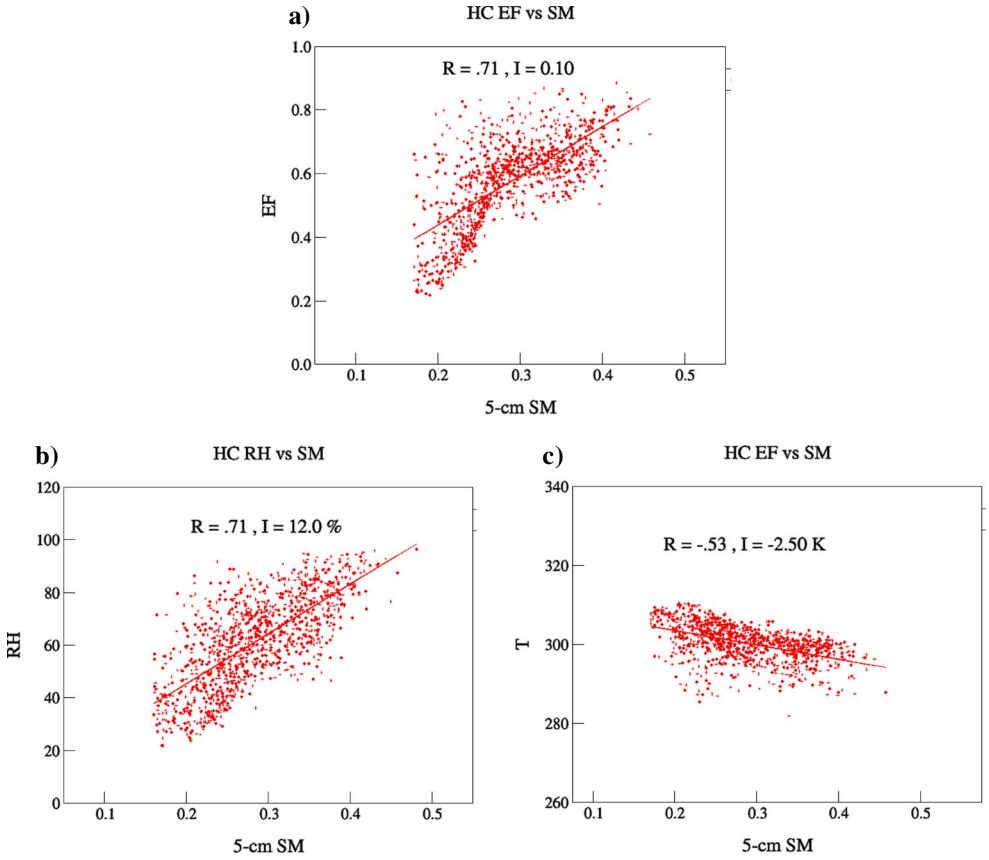

Figure 6. As in Figure 5 except for the controlled HC simulation of the CAM5.1/CLM4 model.

expected in a free-running simulation of this type, the modeled precipitation also does not align well with the timing of the observed events. There is a better correspondence of the timing of modeled and observed *P* events in the HC simulation (a consequence of its more realistic atmospheric and land states); but the simulated amplitudes remain mostly too low: although the HC soil moisture is more realistically initialized each day, it still "feels" the effects of the too scant model precipitation amounts on *intradiurnal* time scales.

While underpredicting precipitation peaks in the observed time series, the accumulated seasonal precipitation in both the AMIP and HC simulations (Figure S3) configurations moderately exceed the observations during the dry 2006 warm season. This disparity appears to result from a pervasive "drizzle effect" (Stephens et al., 2010), wherein climate models are found to rain out in smaller amounts and at higher frequencies than are observed. In the much wetter 2007 warm season, however, both configurations show pronounced shortfalls in accumulated precipitation (in the AMIP run, more than in the HC).

Table 4 summarizes the LAC metrics for the AMIP and HC simulations and compares these with observational values that are linearly averaged over the three SM data sets listed in Table 1. For each LAC metric, the ±95% confidence intervals also are shown in brackets, where it is assumed that the observational averages constitute 164 statistically independent daily soil moisture-atmospheric pairs (the same as that associated with the EBBR SM measurements, which suffered the most missing data). Because there are no missing model data, the corresponding number of statistically independent samples is 221 (every fifth day in a total of 1,107 in MJJA 2003–2011). The AMIP and HC *R* metrics are all much higher than the corresponding observational averages and also are distinguishable with 95% confidence from the latter. In contrast, when comparing the AMIP versus HC correlations, only the SM-T couplings are clearly distinguishable. This suggests that the AMIP-HC differences in SM-T coupling strength may not only be a consequence of the HC's more realistic land state but also may depend on AMIP-HC differences in radiative and hydrological forcings of the land, as well as parameterizations that govern the latent and sensible heat transfers at the soil-atmosphere interface.

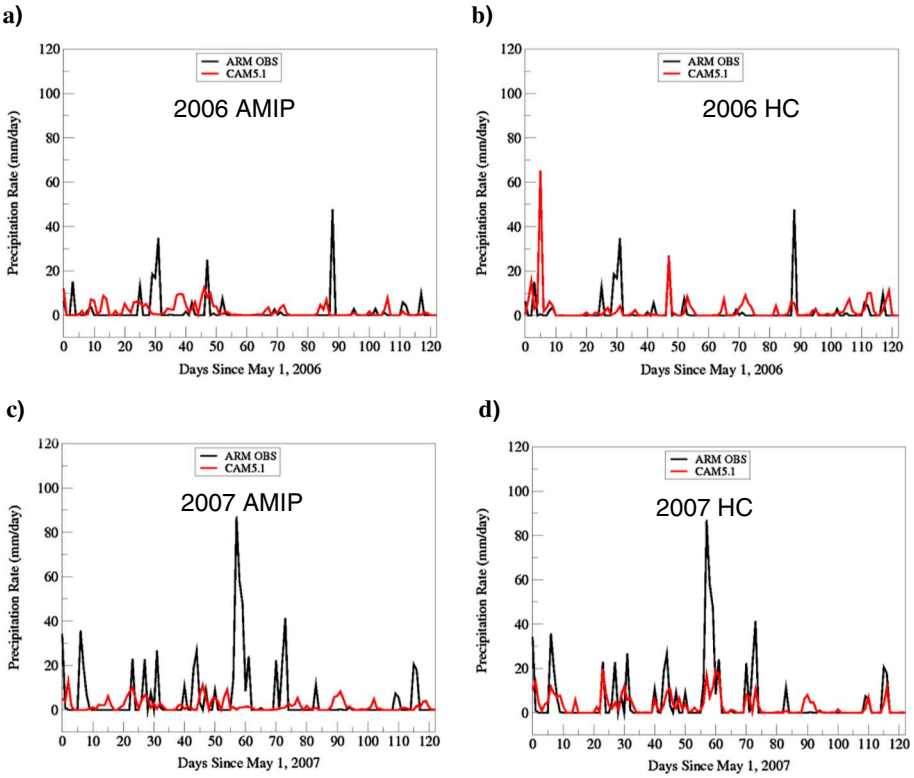

Figure 7. Time series of (a and c) AMIP and (b and d) HC simulations of daily average precipitation rate (in mm d^{-1}, red line) at the closest model grid point to the ARM SGP-CF site (coordinates 36.28°N, 97.50°W) during the MJJA season of relatively dry and wet years 2006/2007. These model results are compared with observations (black line) at the CF site (coordinates 36.61°N, 97.48°W) for the same time periods.

Listed in Table 5 are model performance statistics (mean bias, root-mean-square error (RMSE), and modeled versus observational temporal variance ratio σ_m^2/σ_o^2) of AMIP- and HC-simulated single variables at the near-CF grid point, evaluated relative to ARMBE observations at the CF site. All performance metrics are computed using daily average model and observational values for the 2003–2011 MJJA warm seasons. The evaluated model variables include forcings of the land surface (precipitation, net surface shortwave, and longwave radiative fluxes) and of land response variables (surface latent and sensible heat fluxes, evaporative fraction, surface relative humidity and temperature, and soil moisture at 5 cm depth).

From Table 5, the precipitation rate is negatively biased in both simulations but is less so in the controlled HC configuration, as Figure 7 implies. In both simulations also, the modeled net surface shortwave heating is underpredicted, while the surface net longwave cooling is overpredicted, resulting in an excessive overall radiative cooling of the surface. The controlled HC run shows a lesser radiative cold bias than the AMIP, however.

The surface latent heat flux is negatively biased for both model configurations, while the surface sensible heat flux is biased positive for the AMIP but negative for the HC. These turbulent flux differences yield an evaporative fraction that is smaller than observed for the AMIP run but larger than observed for the HC. Both model configurations display negatively biased surface relative humidity (consistent with underpredicted latent heat fluxes) and positively biased surface air temperature (consistent with overpredicted net upward longwave radiation). Hence, the modeled atmospheric surface layer is systematically too warm and dry, although much more so in the AMIP run than in the HC.

Simulated soil moisture is a model-specific variable (Koster et al., 2009) and so will not necessarily agree closely with observations. For example, the modeled SM at 5 cm depth for both the AMIP and HC simulations is closer to that of the SWATS measurements, which at the CF site do not display as large a range of variation as the CO2FLX data. (The 5 cm soil moisture performance statistics are not calculated relative to EBBR measurements at 2.5 cm depth.) The tendency of the free-running AMIP simulation to frequent drier

Table 4
The Top Table Lists the Arithmetic Average of the Coupling Strength Metrics R *and* I *Associated With the SWATS, CO2FLX, and EBBR Soil Moisture Measurements at the SGP-CF Site (Coordinates 36.61°N, 97.48°W)*

Average observed coupling strength	
SM-EF	R = 0.42 [0.28 to 0.54] I = 0.053
SM-RH	R = 0.45 [0.32 to 0.57] I = 5.86%
SM-T	R = −0.32 [−0.17 to −0.45] I = −1.50 K

Model coupling strengths	AMIP	HC
SM-EF	R = 0.67 [0.57 to 0.75] I = 0.13	R = 0.71 [0.62 to 0.78] I = 0.10
SM-RH	R = 0.76 [0.70 to 0.81] I = 15.6%	R = 0.71 [0.62 to 0.78] I = 12.0%
SM-T	R = −0.80 [−0.75 to −0.84] I = −4.45 K	R = −0.53 [−0.43 to −0.62] I = −2.50 K

Note. The bottom table lists the corresponding R and I metrics for both the free-running AMIP and the controlled HC simulations at the closest model grid point to CF (coordinates 36.28°N, 97.50°W). For both observational and model results, the R and I values are computed from daily averages over months MJJA of the 2003–2011 period. In both cases also, the range of the $\pm 2\sigma$ (95%) confidence levels on R is indicated in brackets, assuming 164 statistically independent pairings for the observational correlations and 221 for the model simulations (see section 3.1 discussion).

soil moisture states than that of the HC results in a substantially lower mean value of SM (0.234 versus 0.281 m^3/m^3).

It is not surprising that RMS errors listed in Table 5 are generally less for the controlled HC configuration than for the free-running AMIP, which cannot be expected to closely reproduce the observed day-to-day variations. Temporal variance ratios σ_m^2/σ_o^2 also are usually more realistic for the HC simulation than for AMIP. The modeled soil moisture variance at CF is similar to that of the CO2FLX observations but is more than twice as high as that for the SWATS observations. (The latter disparity probably can be discounted, since the variability of the SWATS measurements seems anomalously low at the CF site, see Figures 2–4.) However, for several other variables, the modeled variability is either decidedly too large (surface net longwave flux, evaporative fraction, and relative humidity) or too small (precipitation rate, surface net shortwave flux, and surface turbulent fluxes).

From the standpoint of the representation of land-atmosphere coupling, the model's underprediction of both precipitation amplitude and frequency is perhaps the most troubling. These forcing errors impact the soil moisture, the humidity of the boundary layer, and the turbulent fluxes—all key elements for determining LAC strength.

5.2. Model LAC Evaluated at Regional Scale

The LAC strengths of the model in both AMIP and HC configurations at the near-CF grid point are significantly larger than the observational estimates. However, this grid point "represents" a grid box of dimension 0.9° × 1.25°, and so there is a danger of a scale mismatch in such a single-point comparison with observations. A fuller evaluation of the CAM5.1/CLM4 model thus demands examination of its simulation of LAC across the SGP region. Here we compare the SM-EF coupling, central to the terrestrial component of LAC, against the observational estimates of this quantity that are discussed in section 3.2.

Besides the near-CF model grid point (at 36.28°N, 97.50°W), 11 grid boxes span the 3° × 3° latitude/longitude SGP region. In both AMIP and HC simulations also, the MJJA climatological precipitation displays only a weak spatial gradient that is oppositely directed (westward increasing) to that of the observations (eastward increasing). The model-prescribed regional soil types have varying percentages of sand and clay, and the prescribed vegetation cover mostly consists of generic grass and crop plant functional types (Oleson et al., 2010). These prescribed quantities probably are unlikely to fully capture the observed spatial intersite variations in surface characteristics that are listed in Table 3.

Scatterplots of SM-EF covariances for both AMIP and HC simulations at a grid box that is northwest of the near-CF grid point, and for one to its east, are shown in Figure S2. Because these locations roughly correspond to those of the E4 and E12 observational stations, these model plots can be compared with the observed results shown in Figure S1. The model LAC metrics near the E12 location (Figures S2c and S2d) are much greater than those observed at the E12 station (Figures S1c and S1d). Moreover, the observed *differences* in LAC metrics between the E4 and 12 stations (Figures S1a versus S1c, and S1b versus S1d) are absent in the modeled representations (Figures S2a versus S2c, and S2b versus S2d).

SM-EF strength metrics R and I for the free-running AMIP simulation are provided across 11 model grid boxes in Table S2 and for the controlled HC simulation in Table S3. In the AMIP run (Table S2), there is little variation in the R and I values across model grid boxes, in contrast to their pronounced spatial heterogeneity in region-wide observations (Table 3). For the HC simulation (Table S3), there is somewhat more cross-grid heterogeneity, with R values ranging between 0.49 and 0.74 and I values between 0.050 and 0.14. Presumably, this is mostly a consequence of the controls that keep the HC atmospheric and land states more realistic than those in the free-running AMIP simulation.

Both distance-weighted and unweighted regional averages of R and I values are listed in the bottom rows of Tables S2 and S3, along with an estimate of ±95% confidence intervals, given in brackets. These metrics

Table 5
Comparative Performance Statistics for AMIP (Unshaded rows) and HC (Shaded Rows) Simulations of the CAM5.1/CLM4 Model at Its Closest Grid Point (Coordinates 36.28 N, 97.50 W) to the SGP-CF Site (Coordinates 36.28°N, 97.50°W), With Respect to ARM Observations at the SGP-CF Site, Where All Data Are Daily Averages Over the MJJA Warm Seasons of Years 2003–2011

Variable	Observed mean	Model mean	Mean bias	RMSE	σ_m^2/σ_o^2
Precipitation rate (mm d^{-1})	3.11	2.01	−1.04.	10.69	0.12
		2.77	−0.33	10.37	0.37
Sfc net downward shortwave flux (W m^{-2})	233.0	222.0	−11.0	109.0	0.67
		221.0	−12.0	88.0	0.78
Sfc net upward longwave flux (W m^{-2})	62.0	77.0	+15.0	40.0	1.83
		69.0	+7.0	20.0	1.46
Sfc latent heat flux (W m^{-2})	101.0	73.0	−28.	70.0	0.47
		96.0	−5.0	58.0	0.52
Sfc sensible heat flux (W m^{-2})	47.0	57.0	+10.0	60.0	0.55
		41.0	−6.0	54.0	0.36
Sfc evaporative fraction	0.474	0.454	−0.020	0.20	1.54
		0.536	+0.062	0.16	1.20
Sfc relative humidity (%)	65.5	52.3	−13.2	26.0	2.76
		61.1	−4.4	11.7	1.67
Sfc air temperature (K)	297.3	301.5	+4.2	6.4	1.04
		299.5	+2.2	2.9	1.01
5 cm soil moisture, relative to SWATS (m^3/m^3)	0.283	0.234	−0.049	0.085	2.73
		0.281	−0.002	0.049	2.48
5 cm soil moisture, relative to CO2FLX (m^3/m^3)	0.178	0.234	+0.056	0.101	0.85
		0.281	+0.103	0.104	1.12

Note. The listed statistics include each simulation's mean bias and root-mean-square error (RMSE) with respect to the observations, as well as the ratio of the modeled temporal variability to that of the observations (σ_m^2/σ_o^2).

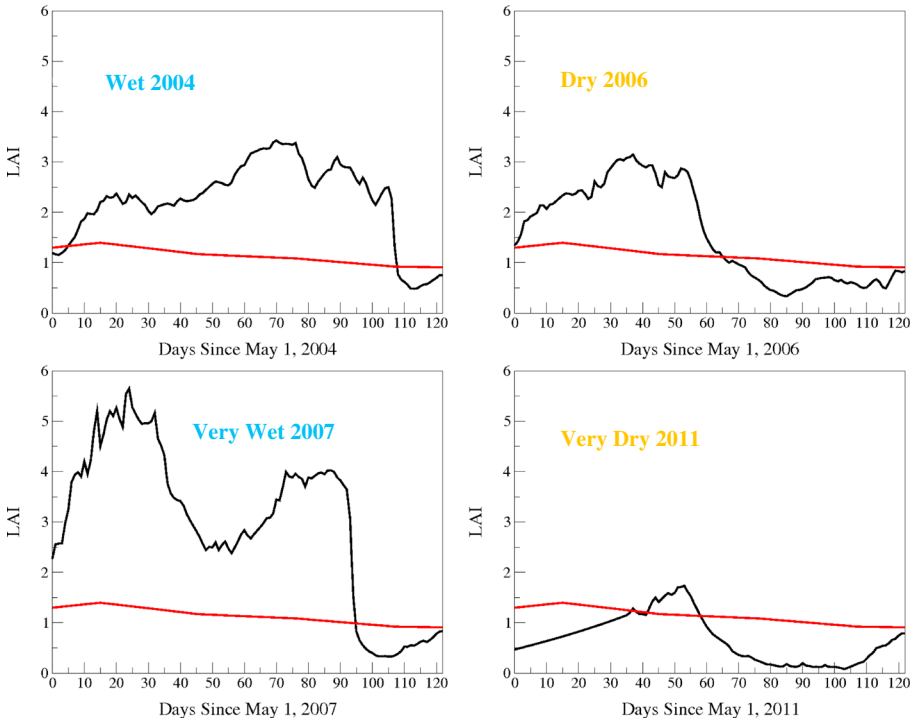

Figure 8. Observational estimates of leaf area index LAI (in dimensionless units) at the SGP-CF site (black lines) in years displaying diverse hydroclimatic conditions, compared with its representation in the controlled HC simulation of the CAM5.1/CLM4 model (red lines) in the same years.

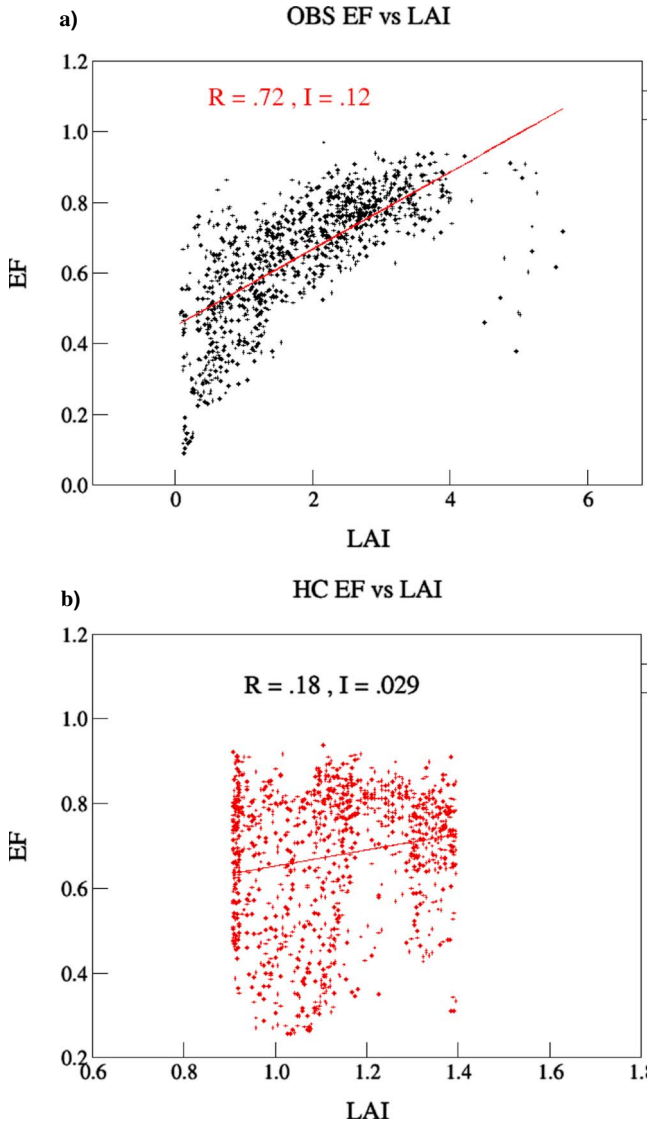

Figure 9. The 2003–2011 MJJA scatterplots and estimated coupling-strength metrics *R* and *I* of local daytime (12 Z to 23 Z) averages of evaporative fraction EF versus leaf area index LAI, as observed (a) at the SGP-CF site for grass land cover and as simulated (b) in the controlled HC experiment of the CAM5.1/CLM4 at the grid point closest to the SGP-CF site.

display little sensitivity to whether a weighted or unweighted averaging procedure is followed. They also are very similar for the AMIP (R = 0.65, I = 0.11–0.12) versus the HC (R = 0.66–0.67, I = 0.10) model configurations. The metrical values all substantially exceed the corresponding observational regional averages (R = 0.27 to 0.35, I = 0.030 to 0.037) listed just below Table 3, and they are statistically distinguishable (with 95% confidence) from the observational averages. Thus, the hypothesis that the modeled SM-EF coupling strengths of the CAM5.1/CLM4 model are too high across the SGP region is confirmed with 95% confidence.

6. Vegetation as an Alternative Coupling Agent

Except over bare-ground areas, the coupling of soil moisture with the surface atmosphere is mediated by vegetation, where the ratio of the local area of the vegetation relative to that of bare ground is commonly expressed by a nondimensional leaf area index (LAI). Williams and Torn (2015) estimated LAI at the grass-covered CF site and at the adjacent wheat field where the CO2FLX instruments are located. They inferred LAI from the normalized difference vegetation index (NDVI) calculated from visible and near-infrared reflectances measured by radiometers at both locations. Williams and Torn (2015) also showed that during daylight hours (when the respective land covers are photosynthetically active, the coupling between LAI and the evaporative fraction EF is markedly stronger than that between 10 cm depth SWATS soil moisture and EF. This is because plant roots tap into soil moisture at greater depths than is immediately available in bare-ground locations, and the evaporative flux associated with transpiration is strongly regulated by vegetation stomatal conductance (proportional to LAI). The mediating vegetation thus plays a larger role in LAC coupling than does the shallow-depth soil moisture at these SGP locations—a result that is also in accord with the regional modeling study of Hirsch et al. (2014) over Australia. The version of CLM4 used in our study does not include dynamic vegetation. Instead, LAI (inferred from satellite measurements of phenology) is prescribed as a seasonal cycle climatology. However, this model prescription does not account for the substantial interannual/intraseasonal variability in LAI that accompanies differences in precipitation amounts and timings during individual warm seasons (see Figure 8). Although the 2003–2011 MJJA mean values of observed versus modeled LAI are of roughly comparable magnitudes (observed mean = 1.88, model mean = 1.14), their interannual/intraseasonal variabilities are very different.

The consequences of these stark differences in LAI variability are illustrated in Figure 9, which contrasts the scatterplot of local daylight averages of EF versus LAI that are observed at the CF site with those simulated by the CAM5.1/CLM4 model at the closest grid point to the CF site. The diminished coherence of the LAI-EF interaction in the model relative to the observational estimate (reflected by much lower model R and I metrics) is striking. However, if the observations of LAI are restricted to the same range as that of the model (LAI values between 0.9 and 1.4—see Figure 8b), the observational LAC strength metrics of Figure 9a are reduced to R = 0.27 and I = 0.030—of the same order as the simulated values R = 0.18 and = 0.029. The model's underestimation of local LAI-EF coupling strength thus seems to be mostly a consequence of the CLM4 prescription of LAI with greatly reduced interannual/intraseasonal range, which does not include observed changes in LAI that depend on the relatively wet or dry character of a particular MJJA warm season (Figure 8).

Using only point observational estimates of LAI in Figures 8a and 9 is, admittedly, not an ideal standard for evaluating the modeled LAI-EF coupling, since a grid point value of LAI represents a spatial average of

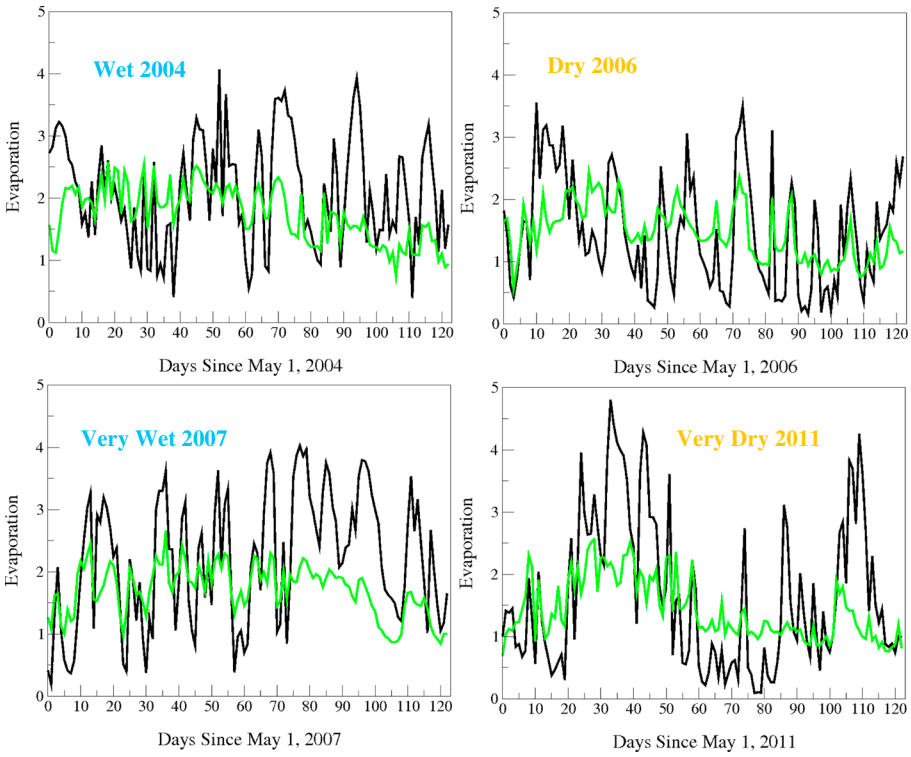

Figure 10. Contributions to surface evaporation E (in units of mm d^{-1}) by vegetation (in green) and by bare soil (in black) in the controlled HC simulation of the CAM5.1/CLM4 model, for the MJJA season in years displaying diverse hydroclimatic conditions. Note that the contributions by vegetation include both transpiration and canopy evaporation.

several different types of land cover that occupy the associated grid box. The estimation of in situ LAI from NDVI requires measurements of spectrally resolved albedo, which are only available currently at the CF site. A fairer in situ test of the modeled LAI-EF coupling at regional scale thus awaits future measurements of spectral reflectance at ARM extended facility sites. Nevertheless, judicious interpretation of Figures 8 and 9 suggests that (1) LAI is an essential complement to shallow-depth soil moisture for estimating terrestrial land-atmosphere coupling strength, and (2) realistic inclusion of the interannual/intraseasonal variability of LAI in models is important for accurately representing this coupling strength (see also Ford & Quiring, 2013 and Zscheischler et al., 2015).

Recent work (Q. Tang, personal communication, 2017) seems to corroborate these assertions. By estimating the regional LAI-EF coupling strength from SGP-downscaled satellite observations of LAI and from EBBR in situ measurements of EF for 2004–2011 warm seasons, the strength of the LAI-EF coupling is found to exceed that of the corresponding shallow-depth SM-EF coupling at six out of eight sites in the SGP region.

Considering the model LAC results of section 3 and taking the implications of Figures 8 and 9 at face value, the CAM5.1/CLM4 appears to overestimate the SM-EF coupling, while underestimating LAI-EF coupling near the CF site. As previously mentioned in our discussion of Figure 6a, these results suggest that more modeled surface evaporation emanates from the bare-ground fraction of the near-CF grid cell than from the vegetated fraction. Figure 10, showing MJJA time series of the model's surface evaporation from bare ground versus vegetation in specific wet and dry years, appears to confirm this hypothesis.

Williams et al. (2016) also found a similar disproportion in the SM-EF versus LAI-EF coupling strengths occurring in a single-column version of the National Center for Atmospheric Research Community Earth System Model (CESM1.2.2) atmosphere, when centered on the SGP-CF site and coupled to the CLM4.5 land model (Oleson et al., 2013). In attempting to correct these coupling biases, Williams et al. (2016) modified selected properties of the CLM4.5 model: they prescribed model LAI according to the

observational estimates of Williams and Torn (2015), while also increasing bare-soil resistance to evaporation, the minimum moisture conductance of vegetation stomata, and leaf reflectance. These modifications improved the single-column model predictions for the warm seasons at the CF site, especially during the dry 2006 summer, when large negative biases in precipitation and positive biases in surface temperature were greatly reduced. Williams et al. (2016) also performed offline CLM4.5 simulations at the CF site, where inputs of the Williams and Torn (2015) LAI estimates were included separately from the modified model physics parameterizations. They found that the LAI and physics changes were approximately of equal importance as potential explanations for the discrepancies between modeled and observed terrestrial coupling metrics.

The performance improvements for the offline CLM and single-column atmospheric model offer some hope for reducing excessive model LAC through physically based alterations of land surface/vegetation characteristics. Of course, implementing similar changes in a more complex climate model such as the coupled CAM5.1/CLM4 may well prove to be a more difficult undertaking (e.g., Hirsch et al., 2016).

7. Concluding Remarks

Our study investigates the terrestrial component of observed land-atmosphere coupling (LAC) at local and regional scales on the U.S. Southern Great Plains (SGP) and its corresponding representation in the CAM5.1/CLM4 coupled atmospheric/land model, when configured in both free-running Atmospheric Model Intercomparison Project (AMIP) and controlled hindcast (HC) simulations.

The main points of this study can be summarized as follows:

1. Different measurements of shallow-depth soil moisture SM reveal considerable variability in observational estimates of LAC and its spatial variability across the SGP region.
2. The spatial variability in observed LAC appears to be associated with an intraregional gradient in the moisture climatology and also to local variations in soil type and land cover.
3. The coupling of surface evaporative fraction with vegetation leaf area index (LAI) is substantially stronger than that with shallow-depth SM, presumably because LAI serves as a proxy for root level soil moisture and plant physiological characteristics that mediate the interaction between soil moisture and surface evapotranspiration.
4. When the CAM5.1/CLM4 model is run in the HC configuration, the biases in simulated forcings and state variables are generally reduced, in comparison with those in the free-running AMIP configuration.
5. To some extent, these HC-AMIP forcing differences act to shift the LAC behaviors of the model, but in both model configurations the SM-EF coupling strength is much greater than the observational estimates, while it displays substantially less spatial variability across the region.
6. In contrast, the coupling of LAI with EF in the model seems too weak at a site where this can be estimated observationally and may be due to an underspecification of LAI interannual/intraseasonal variability and/or to underrepresentation of surface evaporation from the vegetated fraction of the model grid box.

In the discussion that follows, we elaborate on these salient points.

For our study, three alternative choices of Atmospheric Radiation Measurement (ARM) soil moisture observations were available at the SGP-CF site, each having different strengths and weaknesses. An inherent limitation was that only the coupling of atmospheric surface variables with soil moisture at shallow depths (2.5–5.0 cm) could be compared. In future investigations of this type, it would be preferable to estimate observed LAC strengths over a range of depths spanning the vegetation rooting. Hence, it is noteworthy that a successor ARM Soil Temperature and Moisture Profile system measuring soil moisture over five depths at some 17 SGP extended facilities has been deployed since 2015 (Cook, 2016c).

Even for shallow soil depths, considerable uncertainty is evident in observed estimates of LAC strength based on the three different observations of shallow soil moisture. This uncertainty is greatest at the CF site, where artifacts in the reported SWATS soil moisture characteristics make these data markedly different from those of the CO2FLX and EBBR. At each of six ARM extended regional facilities surrounding the CF site, lesser differences in estimated SM-EF LAC strength using SWATS and EBBR soil moistures are found than at the CF site. Spatial variations in LAC strength across the SGP region are substantial, however, due partly to differences in

soil wetness that reflect an observed west-east precipitation gradient across the region; but diverse local soil and land cover types also appear to strongly influence observed regional spatial variability in LAC strength.

With its more realistic atmosphere/land initialization, the controlled HC configuration ameliorates the excessive deviations of the AMIP simulation from SGP-CF observations, but sizeable biases still remain. (The comparison of grid box values to point-wise observations at the CF site introduces some ambiguity in the evaluation of the model performance, however.) The HC simulation's overprediction of variability in evaporative fraction EF and surface relative humidity RH, despite its underprediction of variability in precipitation and surface radiation, implies that the model's excessive terrestrial LAC will not be corrected solely by improving these model forcings. It appears that the detailed physics of the model's interactions among soil moisture, the surface turbulent fluxes, and the surface temperature and humidity states also will need to be improved. The model representation of LAC strength in both the AMIP and HC simulations nonetheless clearly lies outside the envelope of observational uncertainty across the SGP region. Model prediction of overly strong LAC can have significant consequences on a range of time scales: overestimation of the influence of the land on the atmospheric state is likely to produce erroneous weather forecasts, seasonal predictions, and climate change projections.

Another clue as to a possible cause of the deficient representation of LAC by the CAM5.1/CLM4 is provided by considering vegetation LAI as an alternative coupling agent to soil moisture. Compared to the observational evidence (limited to the CF site), the apparently too weak coupling of EF with LAI, and its too strong coupling with soil moisture, suggests that the overly strong representation of LAC may be related to the simulation of evaporation from bare-ground areas, in excess of that from the vegetation cover. Thus, model surface characteristics such as LAI and evaporation resistance parameters, in addition to physical parameterizations of surface fluxes, may also be responsible for the problematic simulation of LAC.

Before CAM/CLM developers can begin to improve the modeled representation of LAC, they will require a more precise, process-oriented diagnosis of the detailed physics of soil moisture and vegetation interactions with surface fluxes and temperature/moisture states. Because of the continual correction of the coupled atmosphere/land state that is implemented in the HC configuration of the model, this simulation lends itself to such a process-oriented investigation. For example, if high-frequency atmospheric observations are available, it is feasible to evaluate *daily* model hindcasts or composites of such hindcasts organized according to synoptic type (e.g., dry- versus wet-day behaviors). Such a fine-grained analysis contrasts with the strictly statistical evaluation of free-running climate simulations that is typically employed. Planned future work therefore will exploit these advantages of the HC model configuration.

We anticipate that LAC studies at different spatiotemporal scales will become increasingly feasible with the advent of soil moisture sensing satellites such as Soil Moisture Ocean Salinity (Kerr et al., 2010) and Soil Moisture Active Passive (Entekhabi et al., 2010), as well as growing networks of in situ data such as International Soil Moisture Network (Dorigo et al., 2011), North American Soil Moisture Database (Quiring et al., 2016), Soil Climate Analysis Network (Strobel et al., 2016, www.wcc.nrcs.usda.gov/scan), and the fledgling National Soil Moisture Network (Strobel et al., 2016). Given that so little is known about the detailed physics of LAC, other studies that pursue diverse diagnostic approaches, and that apply these to different types of models, are to be strongly encouraged.

Acknowledgments
We acknowledge the U.S. Department of Energy (DOE) Atmospheric Radiation Measurement (ARM) program for funding the recording of CO2FLX, EBBR, and SWATS soil moisture and the ARMBE and other atmospheric data sets. The SGP observational data sets used in this study can all be accessed from the ARM archives via the Data Discovery interface at http://www.archive.arm.gov/discovery. Model data used in this study will be made available via a file transfer protocol (ftp) upon request. The work of T. J. P., S. A. K., Y. M., Q. T., and S. X. was funded by the U.S. Department of Energy Office of Science under its ARM, Atmospheric System Research (ASR), and Regional and Global Modeling (RGCM) programs and was performed at the Lawrence Livermore National Laboratory under contract DE-AC52 07NA27344. INW and MST were supported by the U.S. Department of Energy Atmospheric System Research under contract DE-AC02-05CH11231. The work of D. R. C. was funded by the U.S. Department of Energy Office of Science under its ARM Program and was performed at Argonne National Laboratory under contract DE-AC02-06CH11357.

References

Berg, L. K., & Lamb, P. J. (2016). Surface properties and interactions: Coupling the land and atmosphere within the ARM program. In *The Atmospheric Radiation Measurement (ARM) Program: First 20 years, meteorological monographs* (Vol. 57, 23.1–23.17). Boston, MA: American Meteorological Society.

Berg, A., Lintner, B., Findell, K., Seneviratne, S., van den Hurk, B., Cheruy, F., … Gentine, P. (2015). Interannual coupling between summertime surface temperature and precipitation over land: Processes and implications for climate change. *Journal of Climate*, *28*(3), 1308–1328. https://doi.org/10.1175/JCLI-D-14-00324.1

Betts, A. K. (2004). Understanding hydrometeorology using global models. *Bulletin of the American Meteorological Society*, *85*(11), 1673–1688. https://doi.org/10.1175/BAMS-85-11-1673

Betts, A. K. (2009). Understanding land-surface-atmosphere coupling in observations and models. *Journal of Advances in Modeling Earth Systems*, *1*(3), 18. https://doi.org/10.3894/JAMES.2009.1.4

Bond, D. (2005). *Soil Water and Temperature System (SWATS) handbook, ARM Technical Report TR-063* (p. 24). Washington, DC: U.S. Department of Energy.

Bretherton, C. S., & Park, S. (2009). A new moist turbulence parameterization in the Community Atmosphere Model. *Journal of Climate*, *22*(12), 3422–3448. https://doi.org/10.1175/2008JCLI2556.1

Bulmer, M. G. (1979). *Principles of statistics* (p. 252). New York: Dover Publications Inc.
Cheruy, F., Dufresne, J. L., Hourdin, F., & Ducharne, A. (2014). Role of clouds and land-atmosphere coupling in midlatitude continental summer warm biases and climate change amplification in CMIP5 simulations. *Geophysical Research Letters*, *41*, 6493–6500. https://doi.org/10.1002/2014GL061145
Comer, R. E., & Best, M. J. (2012). Revisiting GLACE: Understanding the role of the land surface in land-atmosphere coupling. *Journal of Hydrometeorology*, *13*(6), 1704–1718. https://doi.org/10.1175/JHM-D-11-0146.1
Cook, D. R. (2016a). *Energy Balance Bowen Ratio (EBBR) handbook*, *ARM Tech. Rept. DOE/SC-ARM/TR-037* (p. 24). Washington, DC: U.S. Department of Energy Office of Science.
Cook, D. R. (2016b). *Eddy Correlation Flux Measurement System Instrument handbook*, *ARM Tech. Rept. DOE/SC-ARM/TR-052* (p. 18). Washington, DC: US Department of Energy Office of Science.
Cook, D. R. (2016c). *Soil Temperature and Moisture Profile (STAMP) system handbook*, *ARM Tech. Rept. DOE/SC-ARM-TR-186* (p. 24). Washington, DC: U.S. Department of Energy Office of Science.
Cook, D. R., & Kyrouac, J. (2015). SWATS present and future, presented at the sixth ARM/ASR joint user facility and principal investigator meeting, Vienna, Virginia, March 16–20.
Dirmeyer, P. A. (2001). An evaluation of the strength of land-atmosphere coupling. *Journal of Hydrometeorology*, *2*(4), 329–344. https://doi.org/10.1175/1525-7541(2001)002%3C0329:AEOTSO%3E2.0.CO;2
Dirmeyer, P. A. (2011). The terrestrial segment of soil moisture-climate coupling. *Geophysical Research Letters*, *38*, L16702. https://doi.org/10.1029/2011GL048268
Dirmeyer, P. A., Koster, R. D., & Guo, Z. (2006). Do global models properly represent the feedback between land and atmosphere? *Journal of Hydrometeorology*, *7*(6), 1177–1198. https://doi.org/10.1175/%20JHM532.1
Dirmeyer, P. A., Cash, B. A., Kinter, J. L. III, Stan, C., Jung, T., Marx, L., … Manganello, J. (2012). Evidence for enhanced land-atmosphere feedback in a warming climate. *Journal of Hydrometeorology*, *13*(3), 981–995. https://doi.org/10.1175/JHM-D-11-0104.1
Dirmeyer, P. A., Jin, Y., Singh, B., & Yan, X. (2013). Evolving land-atmosphere interactions over North America from CMIP5 simulations. *Journal of Climate*, *26*(19), 7313–7327. https://doi.org/10.1175/JCLI-D-12-00454.1
Dirmeyer, P. A., Wu, J., Norton, H. E., Dorigo, W. A., Quiring, S. M., Ford, T. W., … Lawrence, D. M. (2016). Confronting weather and climate models with observational data from soil moisture networks over the United States. *Journal of Hydrometeorology*, *17*(4), 1049–1067. https://doi.org/10.1175/JHM-D-15-0196.1
Diro, G. T., Sushama, L., Martynov, A., Jeong, D. I., Verseghy, D., & Winger, K. (2014). Land-atmosphere coupling over North America in CRCM5. *Journal of Geophysical Research: Atmospheres*, *119*, 11,955–11,972. https://doi.org/10.1002/2014D021677
Dorigo, W. A., Wagner, W., Hohensinn, R., Hahn, S., Paulik, C., Drusch, M., … Jackson, T. (2011). The international soil moisture network: A data hosting facility for global in situ soil moisture measurements. *Hydrology and Earth System Sciences*, *15*(5), 1675–1698. https://doi.org/10.5194/hess-15-1675-2011
Entekhabi, D., Njoku, E. G., O'Neill, P. E., Kellogg, K. H., Crow, W. T., Edelstein, W. N., … Van Zyl, J. (2010). The soil moisture active passive mission. *Proceedings of the IEEE*, *98*(5), 704–716. https://doi.org/10.1109/JPROC.2010.2043918
Ferguson, C. R., & Wood, E. F. (2011). Observed land-atmosphere coupling from satellite remote sensing and reanalysis. *Journal of Hydrometeorology*, *12*(6), 1221–1254. https://doi.org/10.1175/2011JHM1380.1
Ferguson, C. R., Wood, E. F., & Vinukollu, R. K. (2012). A global intercomparison of modeled and observed land-atmosphere coupling. *Journal of Hydrometeorology*, *13*(3), 749–784. https://doi.org/10.1175/JHM-D-11-0119.1
Findell, K. L., Gentine, P., Lintner, B. R., & Kerr, C. (2011). Probability of afternoon precipitation in eastern United States and Mexico enhanced by high evaporation. *Nature Geoscience*, *4*(7), 434–439. https://doi.org/10.1038/ngeo1174
Findell, K. L., Gentine, P., Lintner, B. R., & Guillod, B. P. (2015). Data length requirements for observational estimates of land-atmosphere coupling strength. *Journal of Hydrometeorology*, *16*(4), 1615–1635. https://doi.org/10.1175/JHM-D-14-0131.1
Fischer, M. L. (2005). *Carbon dioxide flux measurement systems*, *ARM Technical Report TR-048* (p. 11). Washington, DC: U.S. Department of Energy Office of Science.
Fischer, E. M., Seneviratne, S. I., Luthi, D., & Schar, C. (2007). Contribution of land-atmosphere coupling to recent European summer heat waves. *Geophysical Research Letters*, *34*, L06707. https://doi.org/10.1029/2006GL029068
Fisher, R. A. (1921). On the "probable error" of a coefficient of correlation deduced from a small sample. *Metro*, *1*, 1–3.
Ford, T. W., & Quiring, S. M. (2013). Influence of MODIS-derived dynamic vegetation on VIC-simulated soil moisture in Oklahoma. *Journal of Hydrometeorology*, *14*(6), 1910–1921. https://doi.org/10.1175/JHM-D-13-037.1
Ford, T. W., Rapp, A. D., Quiring, S. M., & Blake, J. (2015). Soil-moisture-precipitation coupling: Observations from the Oklahoma Mesonet and underlying physical mechanisms. *Hydrology and Earth System Sciences*, *19*(8), 3617–3631. https://doi.org/10.5194/hess-19-3617-2015
Ford, T. W., Rapp, A. D., & Quiring, S. M. (2015). Does afternoon precipitation occur preferentially over dry or wet soils in Oklahoma? *Journal of Hydrometeorology*, *16*(2), 874–888. https://doi.org/10.1175/JHM-D-14-0005.1
Ford, T. W., Quiring, S. M., Frauenfeld, O. W., & Rapp, A. D. (2015). Synoptic conditions related to soil moisture-atmosphere interactions and unorganized convection in Oklahoma. *Journal of Geophysical Research: Atmospheres*, *120*, 11,519–11,535. https://doi.org/10.1002/2015JD023975
Ford, T. W., Wang, Q., & Quiring, S. M. (2016). The observation record length necessary to generate robust soil moisture percentiles. *Journal of Applied Meteorology and Climatology*, *55*(10), 2131–2149. https://doi.org/10.1175/JAMC-D-16-0143.1
Ford, T. W., Quiring, S. M., & Frauenfeld, O. W. (2017). Multi-decadal variability of soil moisture-temperature coupling over the contiguous United States modulated by Pacific and Atlantic sea surface temperatures. *International Journal of Climatology*, *37*(3), 1400–1415. https://doi.org/10.1002/joc.4785
Gates, W. L., Boyle, J. S., Covey, C., Dease, C. G., Doutriaux, C. M., Drach, R. S., … Williams, D. N. (1999). An overview of the results of the Atmospheric Model Intercomparison Project (AMIP1). *Bulletin of the American Meteorological Society*, *80*(1), 29–55. https://doi.org/10.1175/1520-0477(1999)080%3C0029:AOOTRO%3E2.0.CO;2
Gentine, P., Entekhabi, D., & Polcher, J. (2011). The diurnal behavior of evaporative fraction in the soil-vegetation-atmospheric boundary layer continuum. *Journal of Hydrometeorology*, *12*(6), 1530–1546. https://doi.org/10.1175/2011JHM1261.1
Gentine, P., Holtslag, A. A. M., D'Andrea, F., & Ek, M. (2013). Surface and atmospheric controls on the onset of moist convection over land. *Journal of Hydrometeorology*, *14*(5), 1443–1462. https://doi.org/10.1175/JHM-D-12-0137.1
Gettelman, A., Liu, A. X., Ghan, S. J., Morrison, H., Park, S., Conley, A. J., … Li, J. L. F. (2010). Global simulations of ice nucleation and ice supersaturation with an improved cloud scheme in the Community Atmosphere Model. *Journal of Geophysical Research*, *115*, D18216. https://doi.org/10.1029/2009JD013797

Guillod, B. P., Orlowsky, B., Miralles, D., Teuling, A. J., Blanken, P. D., Buchmann, N., … Seneviratne, S. I. (2014). Land-surface controls on afternoon precipitation diagnosed from observational data: Uncertainties and confounding factors. *Atmospheric Chemistry and Physics*, *14*(16), 8343–8367. https://doi.org/10.5194/acp-14-8343-2014

Guillod, B. P., Orlowsky, B., Miralles, D. G., Teuling, A. J., & Seneviratne, S. I. (2015). Reconciling spatial and temporal soil moisture effects on afternoon precipitation. *Nature Communications*, *6*, 6443. https://doi.org/10.1038/ncomms7443

Guo, Z., & Dirmeyer, P. A. (2013). Interannual variability of land-atmosphere coupling strength. *Journal of Hydrometeorology*, *14*(5), 1636–1646. https://doi.org/10.1175/JHM-D-12-0171.1

Guo, Z., Dirmeyer, P. A., Koster, R. D., Sud, Y. C., Bonan, G., Oleson, K. W., … Xue, Y. (2006). The global land-atmosphere coupling experiment. Part II: Analysis. *Journal of Hydrometeorology*, *7*(4), 611–625. https://doi.org/10.1175/JHM511.1

Hargrove, W. W., Hoffman, F. M., & Law, B. E. (2003). New analysis reveals representativeness of the AmeriFlux network. *Eos, Transactions American Geophysical Union*, *84*(48), 555.

Hirsch, A. L., Pitman, A. J., & Kala, J. (2014). The role of land cover change in modulating the soil moisture-temperature land-atmosphere coupling strength over Australia. *Geophysical Research Letters*, *41*, 5883–5890. https://doi.org/10.1002/2014GL061179

Hirsch, A. L., Pitman, A. J., & Haverd, V. (2016). Evaluating land-atmosphere coupling using a resistance pathway framework. *Journal of Hydrometeorology*, *17*(10), 2615–2630. https://doi.org/10.1175/JHM-D-15-0204.1

Iacono, M., Delamere, J., Mlawer, E., Shephard, M., Clough, S., & Collins, W. (2008). Radiative forcing by long-lived greenhouse gases: Calculations with the AER radiative transfer models. *Journal of Geophysical Research*, *113*, D13103. https://doi.org/10.1029/2008JD009944

Kerr, Y., Waldteufel, P., Wigneron, J.-P., Delwart, S., Cabot, F., Boutin, J., … Mecklenburg, S. (2010). The SMOS mission: New tool for monitoring key. *Proceedings of the IEEE*, *98*(5), 666–687. https://doi.org/10.1109/JPROC.2010.2043032

Klein, S., Jiang, X., Boyle, J., Malyshev, S., & Xie, S. (2006). Diagnosis of the summertime warm and dry bias over the U.S. Southern Great Plains in the GFDL climate model using a weather forecasting approach. *Geophysical Research Letters*, *33*, L18805. https://doi.org/10.1029/2006GL027567

Koster, R. D., Dirmeyer, P. A., Hahmann, A. N., Ijpelaar, R., Tyahla, L., Cox, P., & Suarez, M. J. (2002). Comparing the degree of land-atmosphere interactions in four atmospheric general circulation models. *Journal of Hydrometeorology*, *3*(3), 363–375. https://doi.org/10.1175/1525-7541(2002)003%3C0363:CTDOLA%3E2.0.CO;2

Koster, R. D., Koster, R. D., Dirmeyer, P. A., Guo, Z., Bonan, G., Chan, E., … Yamada, T. (2004). Regions of strong coupling between soil moisture and precipitation. *Science*, *305*(5687), 1138–1140. https://doi.org/10.1126/science.1100217

Koster, R. D., Sud, Y. C., Guo, Z., Dirmeyer, P. A., Bonan, G., Oleson, K. W., … Xue, Y. (2006). GLACE: The global land-atmosphere coupling experiment. Part I: Overview. *Journal of Hydrometeorology*, *7*(4), 590–610. https://doi.org/10.1175/JHM510.1

Koster, R. D., Guo, Z., Yang, R., Dirmeyer, P. A., Mitchell, K., & Puma, M. J. (2009). On the nature of soil moisture in land surface models. *Journal of Climate*, *22*(16), 4322–4335. https://doi.org/10.1175/2009JCLI2832.1

Koster, R. D., Mahanama, S. P. P., Yamada, T. J., Balsamo, G., Berg, A. A., Boisserie, M., … Wood, E. F. (2010). Contribution of land surface initialization to subseasonal forecast skill: First results from a multi-model experiment. *Geophysical Research Letters*, *37*, L02402. https://doi.org/10.1029/2009GL041677

Koster, R. D., Mahanama, S. P. P., Yamada, T. J., Balsamo, G., Berg, A. A., Boisserie, M., … Wood, E. F. (2011). The second phase of the global land-atmosphere coupling experiment: Soil moisture contributions to subseasonal forecast skill. *Journal of Hydrometeorology*, *12*(5), 805–822. https://doi.org/10.1175/2011JHM1365.1

Koster, R. D., Chang, Y., Wang, H., & Schubert, S. D. (2016). Impacts of local soil moisture anomalies on the atmospheric circulation and on remote surface meteorological fields during boreal summer: A comprehensive analysis over North America. *Journal of Climate*, *29*(20), 7345–7364. https://doi.org/10.1175/JCLI-D-16-0192.1

Kustas, K. P., Hatfield, J. L., & Prueger, J. H. (2005). The soil moisture-atmosphere coupling experiment (SMACEX): Background, hydrometeorological conditions, and preliminary findings. *Journal of Hydrometeorology*, *6*(6), 791–804. https://doi.org/10.1175/JHM456.1

Lamb, P. J., Portis, D. H., & Zangvil, A. (2012). Investigation of large-scale atmospheric moisture budget and land surface interactions over U.S. Southern Great Plains including for CLASIC (June 2007). *Journal of Hydrometeorology*, *13*(6), 1719–1738. https://doi.org/10.1175/JHM-D-12-01.1

Lawrence, D. M., & Slingo, J. M. (2005). Weak land-atmosphere coupling strength in HadAM3: The role of soil moisture variability. *Journal of Hydrometeorology*, *6*(5), 670–680. https://doi.org/10.1175/JHM445.1

Levine, P. A., Randerson, J. T., Swenson, S. C., & Lawrence, D. M. (2016). Evaluating the strength of the land-atmosphere feedback in Earth system models using satellite observations. *Hydrology and Earth System Sciences*, *20*(12), 4837–4856. https://doi.org/10.5194/hess-20-4837-2016

Liu, X., Easter, R. C., Ghan, S. J., Zaveri, R., Rasch, P., Shi, X., … Mitchell, D. (2012). Toward a minimal representation of aerosols in climate models: Description and evaluation in the Community Atmosphere Model CAM5. *Geoscientific Model Development*, *5*(3), 709–739. https://doi.org/10.5194/gmd-5-709-2012

Liu, D., Wang, G., Mei, R., Yu, Z., & Gu, H. (2014). Diagnosing the strength of land-atmosphere coupling at subseasonal to seasonal time scales in Asia. *Journal of Hydrometeorology*, *15*(1), 320–339. https://doi.org/10.1175/JHM-D-13-0104.1

Lorenz, R., Davin, E. L., & Seneviratne, S. I. (2012). Modeling land-climate coupling in Europe: Impact of land surface representation on climate variability and extremes. *Journal of Geophysical Research*, *117*, D20109. https://doi.org/10.1029/2012D017755

Lorenz, R., Pitman, A. J., Hirsch, A. L., & Srbinovsky, J. (2015). Intraseasonal versus interannual measures of land-atmosphere coupling strength in a global climate model: GLACE-1 versus GLACE-CMIP5 experiments in ACCESS1.3b. *Journal of Hydrometeorology*, *16*(5), 2276–2295. https://doi.org/10.1175/JHM-D-14-0206.1

Luo, Y., Berbery, E. H., Mitchell, K. E., & Betts, A. K. (2006). Relationships between land surface and near-surface atmospheric variables in the NCEP North American regional reanalysis. *Journal of Hydrometeorology*, *8*, 1184–1203.

Ma, H.-Y., Chuang, C. C., Klein, S. A., Lo, M.-H., Zhang, Y., Xie, S., … Phillips, T. J. (2015). Evaluation and diagnosis of physical processes in GCMs with an improved hindcast approach: Experiments with specified SST and sea ice. *Journal of Advances in Modeling Earth Systems*, *7*(4), 1810–1827. https://doi.org/10.1002/2015MS000490

Mather, J. H., & Voyles, J. W. (2013). The ARM Climate Research Facility: A review of structure and capabilities. *Bulletin of the American Meteorological Society*, *94*(3), 377–392. https://doi.org/10.1175/BAMS-D-11-00218.1

Mei, R., & Wang, G. (2012). Summer land-atmosphere coupling strength in the United States: Comparison among observations, reanalysis data, and numerical models. *Journal of Hydrometeorology*, *13*(3), 1010–1022. https://doi.org/10.1175/JHM-D-11-075.1

Meng, L., & Quiring, S. M. (2010). Examining the influence of spring soil moisture anomalies on summer precipitation in the U.S. Great Plains using the Community Atmosphere Model version 3. *Journal of Geophysical Research*, *115*, D21118. https://doi.org/10.1029/2010JD014449

Merrifield, A. L., & Xie, S.-P. (2016). Summer U.S. surface air temperature variability: Controlling factors and AMIP simulation biases. *Journal of Climate*, *29*(14), 5123–5139. https://doi.org/10.1175/JCLI-D-15-0705.1

Miralles, D. G., van den Berg, M. J., Teuling, A. J., & de Jeu, R. A. M. (2012). Soil moisture-temperature coupling: A multiscale observational analysis. *Geophysical Research Letters*, *39*, L21707. https://doi.org/10.1029/2012GL053703

Morrison, H., & Gettelman, A. (2008). A new two-moment bulk stratiform cloud microphysics scheme in the NCAR Community Atmosphere Model (CAM3), Part I: Description and numerical tests. *Journal of Climate*, *21*(15), 3642–3659. https://doi.org/10.1175/2008JCLI2105.1

Neale, R. B., Richter, J. H., & Jochum, M. (2008). The impact of convection on ENSO: From a delayed oscillator to a series of events. *Journal of Climate*, *21*(22), 5904–5924. https://doi.org/10.1175/2008JCLI2244.1

Neale, R. B., Chen, C.-C., Gettelman, A., Lauritzen, P. H., Park, S., Williamson, D. L., … Taylor, M. A. (2012). *Description of the NCAR Community Atmosphere Model (CAM5.0)*, *NCAR Technical Note NCAR/TN-486+STR* (p. 274). Boulder, CO: National Center for Atmospheric Research.

Nicholson, S. E. (2015). Evolution and current state of our understanding of the role played in the climate system by land surface processes in semi-arid regions. *Global and Planetary Change*, *133*, 201–222. https://doi.org/10.1016/j.gloplacha.2015.08.010

Notaro, M. (2008). Statistical identification of global hot spots in soil moisture feedbacks among IPCC AR4 models. *Journal of Geophysical Research*, *113*, D09101. https://doi.org/10.1029/2007JD009199

Oleson, K. W., Lawrence, D. M., Bonan, G. B., Flanner, M. G., Kluzek, E., Lawrence, P. J., … Thornton, P. E. (2010). *Technical description of version 4.0 of the Community Land Model (CLM)*, *NCAR Technical Note, NCAR/TN-478+STR* (p. 266). Boulder, CO: National Center for Atmospheric Research.

Oleson, K. W., Lawrence, D. M., Bonan, G. B., Drewniak, B., Huang, M., Koven, C. D., … Yang, Z.-L. (2013). *Technical description of version 4.5 of the Community Land Model (CLM)*, *NCAR Technical Note, NCAR/TN-503+STR* (p. 434). Boulder, CO: National Center for Atmospheric Research.

Orth, R., & Seneviratne, S. (2017). Variability of soil moisture and sea surface temperatures similarly important for warm-season land climate in the Community Earth System Model. *Journal of Climate*, *30*(6), 2141–2162. https://doi.org/10.1175/JCLI-D-15-0567.1

Park, S., & Bretherton, C. S. (2009). The University of Washington shallow convection and moisture turbulence schemes and their impact on climate simulations with the Community Atmosphere Model. *Journal of Climate*, *22*(12), 3449–3469. https://doi.org/10.1175/2008JCLI2557.1

Park, S., Bretherton, C. S., & Rasch, P. J. (2014). Integrating cloud processes in the Community Atmosphere Model, version 5. *Journal of Climate*, *27*(18), 6821–6856. https://doi.org/10.1175/JCLI-D-14-00087.1

Phillips, T. J., & Klein, S. A. (2014). Land-atmosphere coupling manifested in warm-season observations on the U.S. Southern Great Plains. *Journal of Geophysical Research: Atmospheres*, *119*, 509–528. https://doi.org/10.1002/2013JD020492

Phillips, T. J., Potter, G. L., Williamson, D. L., Cederwall, R. T., Boyle, J. S., Fiorino, M., … John Yio, J. (2004). Evaluating parameterizations in general circulation models: Climate simulation meets weather prediction. *Bulletin of the American Meteorological Society*, *85*(12), 1903–1915. https://doi.org/10.1175/BAMS-85-12-1903

Quiring, S. M., Ford, T. W., Wang, J. K., Khong, A., Harris, E., Lindgren, T., … Li, Z. (2016). The North American soil moisture database. *Bulletin of the American Meteorological Society*, *97*(8), 1441–1459. https://doi.org/10.1175/BAMS-D-13-00263.1

Ritsche, M. T. (2008). *Surface Meteorological Observation System handbook*, *ARM Tech. Rept. DOE/SC-ARM TR-031* (p. 31). Washington DC: U.S. Department of Energy Office of Science.

Roundy, J. K., & Santanello, J. A. (2017). Utility of satellite sensing for land-atmosphere coupling and drought metrics. *Journal of Hydrometeorology*, *18*(3), 863–877. https://doi.org/10.1175/JHM-D-16-0171.1

Ruiz-Barradas, A., & Nigam, S. (2006). Great Plains hydroclimatic variability: The view from the North American regional reanalysis. *Journal of Climate*, *19*(12), 3004–3010. https://doi.org/10.1175/JCLI3768.1

Ruiz-Barradas, A., & Nigam, S. (2013). Atmosphere-land surface interactions over the Southern Great Plains: Characterization from pentad analysis of DOE ARM field observations and NARR. *Journal of Climate*, *26*(3), 875–886. https://doi.org/10.1175/JCLI-D-11-00380.1

Santanello, J. A., Friedly, M., & Kustas, W. P. (2005). An empirical investigation of convective planetary boundary layer evolution and its relationship with the land surface. *Journal of Applied Meteorology*, *44*(6), 917–932. https://doi.org/10.1175/JAM2240.1

Santanello, J. A., Friedl, M. A., & Ek, M. B. (2007). Convective boundary layer interactions with the land surface at diurnal time scales: Diagnostics and feedbacks. *Journal of Hydrometeorology*, *8*(5), 1082–1097. https://doi.org/10.1175/JHM614.1

Santanello, J. A., Peters-Lidard, C. D., Kumar, S. V., Alonge, C., & Tao, W.-K. (2009). A modeling and observational framework for diagnosing local land-atmosphere coupling on diurnal time scales. *Journal of Hydrometeorology*, *10*(3), 577–599. https://doi.org/10.1175/2009JHM1066.1

Santanello, J. A., Ferguson, C., Ek, M., Dirmeyer, P., Tuinenburg, O., Jacobs, C., … Lintner, B. (2011). Local land-atmosphere coupling (LoCo) research: Status and results. *GEWEX News*, *21*(4), 7–9.

Santanello, J. A., Peters-Lidard, C. D., & Kumar, S. V. (2011). Diagnosing the sensitivity of local land-atmosphere coupling via the soil moisture-boundary layer interaction. *Journal of Hydrometeorology*, *12*(5), 766–786. https://doi.org/10.1175/JHM-D-10-05014.1

Santanello, J. A., Peters-Lidard, C. D., Kennedy, A., & Kumar, S. V. (2013). Diagnosing the nature of land-atmosphere coupling: A case study of dry/wet extremes in the U.S. Southern Great Plains. *Journal of Hydrometeorology*, *14*(1), 3–24. https://doi.org/10.1175/JHM-D-12-023.1

Santanello, J. A., Roundy, J., & Dirmeyer, P. A. (2015). Quantifying the land-atmosphere coupling behavior in modern reanalysis products over the U.S. Southern Great Plains. *Journal of Climate*, *28*(14), 5813–5829. https://doi.org/10.1175/JCLI-D-14-00680.1

Schneider, J. M., Fisher, D. K., Elliott, R. L., Brown, G. O., & Bahrmann, C. P. (2003). Spatio-temporal variation in soil water: First results from the ARM SGP CART network. *Journal of Hydrometeorology*, *4*(1), 106–120. https://doi.org/10.1175/1525-7541(2003)004%3C0106:SVISWF%3E2.0.CO;2

Seneviratne, S. I., Luthi, D., Litschi, M., & Schar, C. (2006). Land-atmosphere coupling and climate change in Europe. *Nature*, *443*(7108), 205–209. https://doi.org/10.1038/nature05095

Seneviratne, S. I., Corti, T., Davin, E. L., Hirschi, M., Jaeger, E. B., Lehner, I., … Teuling, A. J. (2010). Investigating soil moisture-climate interactions in a changing climate: A review. *Earth-Science Reviews*, *99*(3-4), 125–161. https://doi.org/10.1016/j.earscirev.2010.02.004

Seneviratne, S. I., Wilhelm, M., Stanelle, T., van den Hurk, B., Hagemann, S., Berg, A., … Smith, B. (2013). Impact of soil moisture-climate feedbacks on CMIP5 projections: First results from the GLACE-CMIP5 experiment. *Geophysical Research Letters*, *40*, 5212–5217. https://doi.org/10.1002/grl.50956

Shuttleworth, W. J., Gurney, R. J., Hsu, A. Y., & Ormsby, J. P. (1989). FIFE: The variation in energy partition at surface flux sites. *IAHS Publication*, *186*, 67–74.

Sisterson, D. L., Peppler, R. A., Cress, T. S., Lamb, P. J., & Turner, D. D. (2016). *The ARM Southern Great Plains (SGP) site in the Atmospheric Radiation Measurement (ARM) program: First 20 years*, *Meteorological Monographs* (Vol. 57). Boston, MA: American Meteorological Society.

Snedecor, G. W., & Cochran, W. G. (1967). *Statistical methods* (6th ed., p. 593). Ames, IA: Iowa State University Press.
Song, H.-J., Ferguson, C. R., & Roundy, J. K. (2016). Land-atmosphere coupling at the southern Great Plains atmospheric radiation measurement (ARM) field site and its role in anomalous afternoon peak precipitation. *Journal of Hydrometeorology*, *17*(2), 541–556. https://doi.org/10.1175/JHM-D-15-0045.1
Stephens, G. L., L'Ecuyer, T., Forbes, R., Gettelmen, A., Golaz, J.-C., Bodas-Salcedo, A., … Haynes, J. (2010). Dreary state of precipitation in global models. *Journal of Geophysical Research*, *115*, D24211. https://doi.org/10.1029/2010JD014532
Strobel, M., Lucido, J., Quiring, S., McNutt, C., & Deheza, V. (2016). Building a coordinated national soil moisture monitoring network, presented at the National Soil Moisture Network Workshop, U.S. Department of Agriculture Natural Resources Conservation Service, Boulder, Colorado, 24–26 May.
Sun, J., & Pritchard, M. S. (2016). Effects of explicit convection on global land-atmosphere coupling in the super-parameterized CAM. *Journal of Advances in Modeling Earth Systems*, *8*, 1–22.
Tawfik, A. B., Dirmeyer, P. A., & Santanello, J. A. (2015a). The heated condensation framework. Part I: Description and Southern Great Plains case study. *Journal of Hydrometeorology*, *16*(5), 1929–1945. https://doi.org/10.1175/JHM-D-14-0117.1
Tawfik, A. B., Dirmeyer, P. A., & Santanello, J. A. (2015b). The heated condensation framework. Part II: Climatological behavior of convective initiation and land-atmosphere coupling over the conterminous United States. *Journal of Hydrometeorology*, *16*(5), 1946–1961. https://doi.org/10.1175/JHM-D-14-0118.1
Taylor, C. M., de Jeu, R. A. M., Guichard, F., Harris, P. P., & Dorigo, W. A. (2012). Afternoon rain more likely over drier soils. *Nature*, *489*(7416), 423–426. https://doi.org/10.1038/nature11377
Tuttle, S., & Salvucci, G. (2016). Empirical evidence of contrasting soil moisture-precipitation feedbacks across the United States. *Science*, *352*(6287), 825–828. https://doi.org/10.1126/science.aaa7185
Van Weverberg, K., Morcrette, C. J., Ma, H.-Y., Klein, S. A., & Petch, J. C. (2015). Using regime analysis to identify the contribution of clouds to surface temperature errors in weather and climate models. *Quarterly Journal of the Royal Meteorological Society*, *141*(693), 3190–3206. https://doi.org/10.1002/qj.2603
Wei, J., & Dirmeyer, P. A. (2010). Toward understanding the large-scale land-atmosphere coupling in the models: Roles of different processes. *Geophysical Research Letters*, *37*, L19707. https://doi.org/10.1029/2010GL044769
Wei, J., & Dirmeyer, P. (2012). Dissecting soil moisture-precipitation coupling. *Geophysical Research Letters*, *39*, L19711. https://doi.org/10.1029/2012GL053038
Wei, J., Dirmeyer, P. A., & Guo, Z. (2010). How much do different land models matter for climate simulation? Part II: A decomposed view of land-atmosphere coupling strength. *Journal of Climate*, *23*(11), 3135–3145. https://doi.org/10.1175/2010JCLI3178.1
Williams, I. N., & Torn, M. S. (2015). Vegetation controls on surface heat flux partitioning, and land-atmosphere coupling. *Geophysical Research Letters*, *42*, 9416–9424. https://doi.org/10.1002/2015GL066305
Williams, C. J. R., Allan, R. P., & Kniveton, D. R. (2012). Diagnosing atmosphere-land feedbacks in CMIP5 climate models. *Environmental Research Letters*, *7*(4), 1–9. https://doi.org/10.1088/1748-9326/4/044003
Williams, I. N., Lu, Y., Kueppers, L. M., & Riley, W. J. (2016). Land-atmosphere coupling and climate prediction over the U.S. Southern Great Plains. *Journal of Geophysical Research: Atmospheres*, *121*, 12,125–12,144. https://doi.org/10.1002/2016JD025223
Xie, S. C., McCoy, R. B., Klein, S. A., Cederwall, R. T., Wiscombe, W. J., Clothiaux, E. E., … Turner, D. D. (2010). ARM climate modeling best estimate data: A new product for climate studies. *Bulletin of the American Meteorological Society*, *91*(1), 13–20. https://doi.org/10.1175/2009BAMS2891.1
Xie, S. C., McCoy, R. B., & Tang, Q. (2014). ARM Best Estimate (ARMBELAND) Southern Great Plains central facility (C1) dataset. Retrieved from http://www.arm.gov/data/eval/78, Atmospheric Radiation Measurement (ARM) Climate Research Facility Data Archive.
Zeng, X., & Decker, M. (2009). Improving the numerical solution of soil moisture-based Richards equation for land models with a deep or shallow water table. *Journal of Hydrometeorology*, *10*(1), 308–319. https://doi.org/10.1175/2008JHM1011.1
Zeng, X., Zhao, M., & Dickinson, R. E. (1998). Intercomparison of bulk aerodynamic algorithms for the computation of sea surface fluxes using the TOGA COARE and TAO data. *Journal of Climate*, *11*(10), 2628–2644. https://doi.org/10.1175/1520-0442(1998)011%3C2628:IOBAAF%3E2.0.CO;2
Zeng, X., Barlage, M., Castro, C., & Fling, K. (2010). Comparison of land-precipitation coupling strength using observations and models. *Journal of Hydrometeorology*, *11*(4), 979–994. https://doi.org/10.1175/2010JHM1226.1
Zhang, G. J., & McFarlane, N. A. (1995). Sensitivity of climate simulations to the parameterization of cumulus convection in the Canadian Climate Centre general circulation model. *Atmosphere-Ocean*, *33*(3), 407–446. https://doi.org/10.1080/07055900.1995.9649539
Zhou, Y., Wu, D., Lau, W. K.-M., & Tao, W.-K. (2016). Scale dependence of land-atmosphere interactions in wet and dry regions as simulated with NU-WRF over the southwestern and south-Central United States. *Journal of Hydrometeorology*, *17*(8), 2121–2136. https://doi.org/10.1175/JHM-D-16-0024.1
Zscheischler, J., Orth, R., & Seneviratne, S. I. (2015). A submonthly database for detecting changes in vegetation-atmosphere coupling. *Geophysical Research Letters*, *42*, 9816–9824. https://doi.org/10.1002/2015GL06656